Deformation of the nucleus by TGFβ1 via the remodeling of nuclear envelope and histone isoforms

Ya-Hui Chi (ychi@nhri.org.tw)
National Health Research Institutes https://orcid.org/0000-0002-9216-0938
Wan-Ping Wang
National Health Research Institutes Institute of Biotechnology and Pharmaceutical Research
Ming-Chun Hung
National Health Research Institutes Institute of Biotechnology and Pharmaceutical Research
Gunn-Guang Liou
National Taiwan University College of Medicine
Jing-Ya Wang
National Health Research Institutes Institute of Biotechnology and Pharmaceutical Research
Pen-Hsiu Grace Chao
National Taiwan University

Research Article

Keywords: Nuclear envelope, nuclear lamina, nuclear morphology, TGFβ1

Posted Date: July 29th, 2021

DOI: https://doi.org/10.21203/rs.3.rs-735722/v1

Version of Record: A version of this preprint was published at Epigenetics & Chromatin on January 4th, 2022. See the published version at https://doi.org/10.1186/s13072-021-00434-3.

Deformation of the nucleus by TGFβ1 via the remodeling of nuclear envelope and histone isoforms

Ya-Hui Chi[1,2*], Wan-Ping Wang[1], Ming-Chun Hung[1], Gunn-Guang Liou[3], Jing-Ya Wang[1] and Pen-Hsiu Grace Chao[4]

[1]Institute of Biotechnology and Pharmaceutical Research, National Health Research Institutes, Zhunan, Miaoli County 35053, Taiwan; [2]Graduate Institute of Biomedical Sciences, China Medical University, Taichung 40402, Taiwan; [3]National Taiwan University College of Medicine, Taipei 10051, Taiwan; [4]Department of Biomedical Engineering, School of Medicine and School of Engineering, National Taiwan University, Taipei 10617, Taiwan.

Running title: Nuclear shape linked to TGFβ1 signaling

Keywords: Nuclear envelope, nuclear lamina, nuclear morphology, TGFβ1

* Corresponding author

Ya-Hui Chi

ORCID: 0000-0002-9216-0938

35 Keyan Road, Zhunan, Miaoli County 35053, Taiwan

Ph: +886-37-206166ext35718; Fax: +886-37-586456

Email: ychi@nhri.edu.tw

Abstract

The cause of nuclear shape abnormalities which are often seen in pre-neoplastic and malignant tissues is not clear. In this study we report that deformation of the nucleus can be induced by TGFβ1 stimulation in several cell lines including Huh7. In our results, the upregulated histone H3.3 expression downstream of SMAD signaling contributed to TGFβ1-induced nuclear deformation, a process of which requires incorporation of the nuclear envelope (NE) proteins lamin B1 and SUN1. During this process, the NE constitutively ruptured and reformed with no observable indications of DNA damage response. Contrast to lamin B1 which was relatively stationary around the nucleus, the upregulated lamin A was highly mobile, shuttling between the nucleus and cytoplasm, and clustering at the nuclear periphery. The chromatin regions that lost NE coverage formed a supra-nucleosomal structure characterized by elevated histone H3K27me3 and histone H1, the formation of which depended on the presence of lamin A. These results provide evidence that shape of the nucleus can be modulated through TGFβ1-induced compositional changes in the chromatin and nuclear lamina.

Introduction

The cell nucleus is a double membrane-enclosed organelle. Most nuclei appear spheroid or ellipsoid; however, the shape can vary from trilobed in human neutrophils to dumbbell-shaped in some white blood cells. Nuclear atypia which refers to abnormally-shaped cell nuclei is a term used in cytopathology, and is considered a significant indicator of malignancy [1]. The morphology of the cell nucleus is also a key indicator of the disease state and prognosis of progeria, neurodegenerative diseases and virus infection [2-7]. Changes in nuclear shape have been linked to chromatin reorganization and gene expression [5, 8]; however, the molecular signaling underlying the variations in nuclear morphology has yet to be elucidated.

The nuclear lamina beneath the inner nuclear membrane is a meshwork of type V intermediate filament proteins consisting primarily of A- and B- type lamins [9]. The expression of B-type lamins is relatively constant among tissues, whereas the abundance of lamin A vary systematically by as much 30-fold between soft and stiff tissue. High lamin A levels can physically stabilize the nucleus against stress and thereby protect the nuclear lamina and chromatin. It is suggested that the mechanical signals transmitted from the extracellular environment to the nucleus mediated by the cytoskeleton may fine tune the lamin A:B for cell-specific gene expression [10]. Abnormalities in the nuclear lamina are

hallmarks of many human diseases [11]. Different types of lamina abnormality, such as herniations, honeycomb-like structures, and irregular staining, have been observed in primary dermal fibroblasts derived from *LMNA*-variant carriers [12]. These findings indicate that the level and composition of nuclear lamins in different tissues must be fine-tuned in a manner that prevents rupturing of the NE without constraining migration [13].

Cancer cells utilize epithelial-mesenchymal transition (EMT) in the migration from their epithelial cell community and integration into tissue at remote locations (i.e., distant metastasis). This switch in cell differentiation and behavior is mediated by changes in cell morphology as well as post-transcriptional and post-translational gene regulation [14, 15]. Whereas changes in cell shape are linked to local gradients in signaling molecules for the subsequent cell activities [16], the means by which the nuclear shape is regulated in response to extracellular signaling remains unclear. In this study, we discovered that shape of the nucleus became highly deformed under the treatment of TGFβ1. The nuclear envelope (NE) proteins SUN1 and the B-type lamin, and the SMAD-downstream upregulation of a histone H3 variant H3.3, are required for this process. Whereas the A-type lamin is dispensable for the TGFβ1-induced nuclear deformation, it is recruited to enclose the NE after the rupture, as well as the clustering of H3K27me3 and histone H1.

These results provide evidence that nuclear shape is linked to TGFβ1 signaling involved in the compositional remodeling of the nuclear lamina, core histones, and linker histones.

Results

Deformation of nuclear morphology induced by TGFβ1

Transforming growth factor beta 1 (TGFβ1) is a pleotropic cytokine essential to a variety of cellular functions, including EMT. We serendipitously discovered that the nuclear morphology of Huh7 hepatocellular carcinoma cells became abnormally shaped when treated with TGFβ1 (Fig. 1A), concomitant with increases in the expression of mesenchymal markers N-Cadherin and Vimentin (Fig. 1B). The nuclear morphology gradually deformed over time, with more than 70% of the nuclei becoming non-ovoid after two days of TGFβ1 treatment (Fig. 1, A and C and Supplementary Fig. S1A). Live-cell imaging of fluorescent histone H2B revealed that the nuclear shape was more dynamic in TGFβ1-treated than in mock-treated cells (Fig. 1D, Supplementary movie S1 and movie S2). Measured at intervals of 30 minutes post-treatment, the percent change was roughly 60% higher in TGFβ1-treated cells than in mock-treated cells (Fig. 1, E and F). Using elliptic Fourier analysis (EFA) to compute elliptic axial ratios (ARs) describing the nuclear shape [17], we identified a drastic increase in shape abnormalities in TGFβ1-treated nuclei (Fig. 1, G and H). TGFβ1-induced nuclear shape aberrations were also observed in RD (human rhabdomyosarcoma), NMuMG (mouse mammary gland epithelial cell), and HT-1080 (human fibrosarcoma) cells (Supplementary Fig. S1B). These results revealed that

morphology of the nucleus becomes highly deformed under TGFβ1 stimulation, an observation similar to nuclear atypia occurs in malignant tissues.

Nuclear envelope (NE) proteins differ in their contributions to TGFβ1-induced nuclear deformation

The nuclear lamina provides mechanical support to the nucleus via interactions with the LINC (linker of nucleoskeleton and cytoskeleton) complex comprising SUN (Sad1 and UNC84)-domain proteins and proteins that contain spectrin repeats [18, 19]. Thus, we sought to determine whether nuclear lamins and/or inner nuclear membrane (INM) proteins participate in TGFβ1-induced nuclear deformation. Knocking down lamin B1 or SUN1 using siRNAs modestly reduced the expression of mesenchymal markers N-Cadherin and Vimentin in cells stimulated by TGFβ1 to undergo EMT, and the nuclei remained ovoid-like. Conversely, the depletion of lamin A, SUN2, or Emerin had no effect on Vimentin expression or TGFβ1-elicited aberrancies in nuclear morphology (Fig. 2, A-C). On the other hand, knocking down lamin B1 or SUN1 two days after TGFβ1 treatment abolished the induced deformation of the nucleus (Supplementary Fig. S2, A-C). These results indicate that the mechanical forces transmitting through lamin B1 and SUN1 independently contribute to TGFβ1-induced changes in nuclear shape, regardless of the occurrence of EMT.

The immunofluorescence staining images revealed that a portion of the chromatin in cells treated with TGFβ1 lost coverage of both A- and B-type lamins (i.e. NE rupture, Fig. 2, D and E, yellow stars in Fig. 2E). A closer examination of the images revealed that part of the nucleus was stained negative for lamin B but positive for lamin A, the immunofluorescence signal of which was significantly higher following TGFβ1 treatment (white arrow heads in Fig. 2E). Western blot analysis showed that TGFβ1 provoked a significant increase in the expression of lamin A/C, but not lamin B1 or other INM proteins (e.g. SUN1, SUN2 and Emerin; Supplementary Fig. S3, A and B). In the presence of TGFβ1, SUN1 and FG domain-containing nuclear pore complex (NPC) proteins overlapped more with lamin B than lamin A (Supplementary Fig. S3, C and D), whereas Emerin co-localized more with lamin A (Supplementary Fig. S3E).

Differential mobility of lamin A and lamin B1 during TGFβ1-induced nuclear deformation

We subsequently followed the localization of lamin A in real time. Lamin A, which was initially distributed homogenously within the nucleus, became partially disassembled and leaked into the cytoplasm (Fig. 3A, compare times 0’ and 20’, Supplementary movie S3). Within 10 minutes after the rupture, lamin A clusters appeared at the junction between the nucleus and cytoplasm, and then redistributed homogeneously throughout the nucleus (Fig.

3A, compare times 150' and 440'). During this process, the nucleus in each cell expanded and regressed in size multiple times (Fig. 3B and Supplementary movie S3). Live-cell imaging also revealed that the chromatin region covered with lamin A and devoid of lamin B1 was more mobile than the chromatin region covered with both lamin A and lamin B1 (Fig. 3C and Supplementary movie S4).

Using a nuclear-localizing green fluorescent protein (i.e. GFP-NLS) to track the localization of nuclear-residing proteins during TGFβ1-induced nuclear deformation, it was found that GFP-NLS leaked into the cytoplasm at the time of lamin A disassembly (Fig. 3D and Supplementary movie S5). As the clustered lamin A re-integrated into the nucleus, GFP-NLS was gradually imported from the cytoplasm into the nucleus (Fig. 3, D and E). We further created a *LMNA*-knockout cell line (i.e., LMNA_KO) using the CRISPR/Cas9 method to verify the role of lamin A in the nuclear deformation process (Supplementary Fig. S3F). Similar to the results obtained using RNAi (Fig. 2B), the nuclear morphology of LMNA_KO cells deformed after TGFβ1 treatment (Supplementary Fig. S3G); however, nuclear-localizing GFP did not shuttle back to the nucleus once leaked into the cytoplasm (Fig. 3, F and G; Supplementary move S6), indicating that lamin A is dispensable to the rupture, but crucial to the integrity of the NE during reformation. Intermittent, non-lethal ruptures of the nuclear envelope have been observed in dermal

fibroblasts derived from patients of laminopathies and in *Lmna* knockout mouse embryonic fibroblasts [20]. The TGFβ1-induced rupture and deformation of the NE observed here should be different from the NE rupture events in *Lmna*-deficient cells due to the intactness of the nuclear lamina prior to TGFβ1 stimulation.

Denais et al. and Raab et al. reported that DNA double-strand breaks coincide with NE opening events. They observed that small pieces of the nuclear material pinched off from the primary nucleus as cells passed through narrow constrictions, which increased the number of nuclear fragments positive for γH2AX [21, 22]. However, γH2AX immunofluorescence staining in this study did not reveal evidence of elevated DNA damage response in cells treated with TGFβ1 (Supplementary Fig. S4). These results suggest that TGFβ1-induced NE rupture is not accompanied with breaks in DNA.

Upregulation of histone H3.3 downstream of SMAD signaling is required for TGFβ1-induced nuclear deformation

We sought to determine whether phosphorylation of the receptor-activated (R)-SMAD family is required for TGFβ1-induced nuclear deformation. We found that shape of the nucleus remained ovoid in the presence of SB-431542, a selective inhibitor of TGF-βRI blocking phosphorylation of the SMAD complex. Removal of TGFβ1 at 24 hours after the addition of TGFβ1 had no effect on the tendency toward nuclear deformation (Fig. 4, A-

C). Knocking down SMAD2 or SMAD3 using siRNAs reduced the extent of nuclear morphology alteration (Supplementary Fig. S5, A-C), whereas overexpressing SMAD2 (tagged with HA) was sufficient to trigger deformation of the nucleus in the absence of TGFβ1 (Supplementary Fig. S5D, denoted by white arrow head). These results indicate that SMAD-downstream signaling contributes to TGFβ1-elicited nuclear deformation; removal of extracellular TGFβ1 failed to restore the nuclear shape once the process is initiated.

The rigidity of chromatin is closely associated with the epigenetic status of the histone tails [23, 24]. Thus, we adopted a proteomic strategy to identify novel epigenetic modifications of histone H3 under TGFβ1 treatment (Fig. 4D). No significant differential epigenetic modification was detected (Supplementary Table S1). Rather, our LC-MS/MS results revealed that the protein level of histone H3.3 increased by roughly 2.6-fold following the treatment with TGFβ1 (Supplementary Table S2). This observation was verified by Western blot analysis and qRT-PCR of *H3-3A* (i.e., the H3.3 gene, Fig. 4, E and F). Knocking down *H3-3A* using siRNAs abolished both TGFβ1-induced EMT and nuclear deformation (Fig. 4, F-H). Furthermore, depleting SMAD2 or SMAD3 reduced the transcription of *H3-3A* (Fig. 4E). These findings indicate that the deformation of nuclear morphology induced by TGFβ1 is a SMAD-downstream event following the upregulation

of H3.3.

Enrichment of histone H1 and H3K27me3 at chromatin regions that lost NE coverage

We next sought to identify the epigenetic modification(s) of histones associated with NE rupture. Using antibodies that recognize specific epigenetic modifications of histones, we discovered that the immunofluorescence signals of H3K27me3 and H1 were well correlated, and enhanced in chromatin regions that had lost lamin B upon TGFβ1 stimulation (Fig. 5A and Supplementary Fig. S6A). Immunofluorescence staining revealed that the intensity of H3K27me3 was strongly correlated with H3.3 localization in cells subjected to TGFβ1 treatment (Fig. 5B). The distribution of H3K27me3 was shown not to overlap with H3K9me3, both of which are markers for heterochromatin (Fig. 5C) [8]. In transmission electron microscopic (TEM) images, heterochromatin generally appears as small, darkly stained, irregular particles scattered throughout the nucleus or accumulated adjacent to the NE. We used immunogold labeling to characterize the ultrastructural organization of subcellular features of the chromatin associated with H3K27me3 enrichment at nanoscale. The chromatin regions labeled with H1 (indicated by the red arrow head) and H3K27me3 (indicated by the blue star) appeared less dark in TGFβ1-treated cells than in untreated cells, which is indicative of lower chromatin packing density

(Fig. 5D).

The monoclonal histone H1 antibody in Figure 5A recognized the histone H1 variants H1.4 and H1.5. When using RNAi, it was found that the depletion of either H1.4 or H1.5 ameliorated TGFβ1-induced nuclear deformation, and the NE remained intact (Fig. 5, E and F). The nucleus of cells depleted for H1.4 or H1.5 did not present an ovoid morphology; however, the degree of deformation was lessened, as evidenced by the AR ratios (Fig. 5, F and G). By contrast, the TGFβ1-induced nuclear morphology was unaffected by the depletion of H1.2 or H1.3 (Supplementary Fig. S6, B and C). These results suggest that incorporation of specific variants of linker histone H1 occur prior to the NE rupture.

Lamin A contributes to TGFβ1-induced clustering of histone H1 and H3K27me3

There have been reports of lamin A/C interacting with the Polycomb group (PcG) of proteins, such as EZH2, for their nuclear compartmentalization and transcriptional regulation [25, 26]. Therefore, we sought to determine whether lamin A is involved in the localization of H3K27me3 in Huh7 cells stimulated using TGFβ1. In LMNA_KO Huh7 cells, we did not observe significant clustering of H3K27me3 or histone H1 in the chromatin regions of TGFβ1-induced deformed nuclei that lost lamin B coverage (Fig. 6A). To determine whether *LMNA* depletion alters the association between H3K27me3 and

histone H1, we used a proximity ligation assay (PLA), which permits the detection of transient interactions occurring between two proximal proteins separated by <30 nm (Fig. 6, B and C) [27]. Our results revealed that H3K27me3 was in close proximity with histone H1 in TGFβ1- as well as mock-treated cells, and the incidence of the associations increased by roughly 3.3-fold following TGFβ1 treatment ($P < 0.001$). In the presence of TGFβ1, there was no difference in the number of PLA dots in LMNA_KO cells and LMNA_WT cells ($P = 0.8936$); however, the average integrated intensity of each dot within a cell was significant lower ($P < 0.001$) in LMNA_KO than in LMNA_WT cells (Fig. 6, D and E). Together with the observation in immunofluorescence staining and immunogold TEM images (Fig. 5, A and D), these results suggest that lamin A is not essential to the association between H3K27me3 and histone H1, but rather contributes to the formation of a supra-nucleosomal structure enrich with H3K27me3 and histone H1 upon TGFβ1 stimulation.

Discussion

Abnormalities in nuclear morphology are hallmarks of many diseases, including progeria and cancer [28]. In the current study, we discovered that the multifunctional growth factor TGFβ1 alters the nuclear shape and induces NE rupture in a specific cell line subset. This cellular phenotype is a downstream signaling of SMAD2/3 phosphorylation, which requires the upregulation of histone H3.3 and the mechanical force link to nuclear lamin B1 and SUN1. We observed a strong correlation between the distribution of histones H1 and the H3K27me3 epigenetic mark in regions of chromatin that lost NE coverage, and this association is lamin A dependent. This led us to propose a biophysical model in which TGFβ1 signaling initially increases the expression of H3.3 for the subsequent transcription of EMT genes, followed by the incorporation of specific histone H1 variants and H3K27me3 epigenetic mark for nuclear deformation and NE rupture (Fig. 7).

The means by which the nucleus alters its morphology to allow cells to cross physical barriers and migrate through confined spaces has been investigated [29-31]. In studies on the migration of the nucleus through tight spaces, the incidence of NE rupture was shown to increase with cell confinement and the depletion of nuclear lamins [21, 22]. In those reports, opening of the NE allowed nuclear proteins to leak out of the nucleus and cytoplasmic proteins to leak in. Note that DNA double-strand breaks coincided with NE

opening events, and ESCRT (endosomal sorting complexes required for transport)-dependent DNA repair is crucial to cell survival [21, 22]. In the current study, we also observed the nucleo-cytoplasmic shuttling of nuclear content upon constitutive rupture and reformation of the NE induced by TGFβ1 (Fig. 3, D and E). However, we did not find any signaling indicative of DNA damage (Supplementary Fig. S4). These results suggest that the TGFβ1-initiated signal cascade associated with nuclear deformation differs from the spontaneous deformations associated with cell migration through confined spaces.

Laminopathies that feature deformed nuclei are caused by mutations in *LMNA* [2]; however, the TGFβ1-induced nuclear deformation in this study was shown to depend on the presence of SUN1 and lamin B1, but not lamin A (Fig. 2, B and C). Note that SUN1 co-localized with lamin B, but not with clustered lamin A (Supplementary Fig. S3C). There are inherent differences in the structures formed by A- and B-type lamins in the lamina and nucleoplasm [32]. Lamin B1 but not lamin A tends to be weak or absent at nuclear membrane protrusions (or blebs) [21, 32-35]. We also observed differences in the expression levels and localization of lamin A and lamin B1 upon TGFβ1 stimulation (Fig. 2E and Supplementary Fig. S3A). Interestingly, the chromatin regions with lamin A coverage but without nuclear lamin B1 coverage gained more mobility than did the chromatin regions covered with both lamin A and lamin B1 (Fig. 3C). Moreover, the

depletion of lamin A prevented recovery of GFP-NLS in the nucleus upon TGFβ1-induced rupturing of the NE (Fig. 3, F and G). These evidences suggest that lamin A and lamin B1 play different roles in regulating the nuclear shape; however, they are both required for closure of the NE following rupture.

Lamin A levels directly or indirectly regulate many proteins involved in tissue-specific gene expression. TGFβ1 is a strong stimulator of collagen secretion [36], and lamin A responds to collagen levels, which scale with tissue stiffness [10]. In addition, lamin A/C modulates cellular responses to TGFβ1 signaling on collagen production [37]. In previous research, lamin A/C-rich NE blebs appeared condensed with transcriptionally active histone marks in lamin B2-deficient cells [32]. Lamin A/C has been discovered evolutionarily required for correct PcG-mediated nuclear compartmentalization and higher-order structures [26]. In the current study we observed that *LMNA* depletion significantly reduced the TGFβ1-induced clustering of H3K27me3 and H1 (Fig. 6). It is likely that the lodging and dislodgement of lamin A within the chromatin may facilitate the formation and disassembly of the supra-nucleosomal structure associated with TGFβ1-induced transcriptional regulation.

In the current study, we found that the incorporation of histone H1, H3.3 and the H3K27me3 epigenetic mark was higher in regions of chromatin that herniated through the

NE (Fig. 5, A-B). Replacing canonical histones with histone variants in the nucleosome has previously been shown to modify chromatin structure and gene expression [38]. The histone variant H3.3 maintains a decondensed chromatin state, and has been implicated in the balance between open and condensed chromatin, which is crucial to the fidelity of chromosome segregation during early mouse development [39]. H3.3 deposition has long been associated with gene activation; however, one genome-wide profiling study reported that H3.3 may facilitate a dynamic chromatin environment that allows for optimal PRC2 binding and activity, thereby promoting the establishment of a bivalent chromatin landscape in embryonic stem cells (ESCs) [40]. B-type lamins are closely associated with repressive chromatin [41]; therefore, our observation of H3.3 and H3K27me3 co-localization in chromatin regions devoid of nuclear lamin B indicates that TGFβ1 may initiate a cascade of gene transcription activities requiring the dislodgement of B-type lamins. Identifying the mechanism by which the nuclear lamins coordinate with histone variants for gene regulation in response to TGFβ1 will require further investigation [42, 43].

Members of the linker histone H1 family bind to nucleosomal core particles around DNA entry and exit sites, and stabilize both the nucleosome structure and higher-order chromatin architecture [44]. H1 has long been seen as a general condenser of chromatin

[45]; however, there is a growing body of evidence indicating that H1 has the potential to fine-tune transcription in a locus-specific manner [46, 47]. In this study, we discovered a subtype-specific (i.e., H1.4 and H1.5) requirement of histone H1 for the TGFβ1-induced nuclear deformation (Fig. 5, E-G). The existence of multiple H1 subtypes and various posttranslational modifications adds to the complexity and challenges associated with studying this protein family [44, 48]. The collaboration of H1 subtype members with core histones in gene regulation would depend on the availability of antibodies that recognize specific subtypes of histone H1.

In summary, we discovered a novel phenotype involved in deformation of the nucleus under the effects of TGFβ1 signaling. The rupturing and reformation of the NE require multiple consecutive changes in the composition of the nuclear lamina as well as core and linker histones. These results reveal a molecular mechanism that renders the morphology of the nucleus responsive to TGFβ1 signaling, which plays a crucial role in tissue homeostasis and disease progression.

Materials and Methods

Cell culture

Huh7 hepatocellular carcinoma cell line was sourced from JCRB cell bank (JCRB0403, Japan). Huh7, RD (CCL-136, ATCC, VA, USA) and NMuMG (CRL-1636, ATCC) cell lines were maintained in high glucose Dulbecco's Modified Eagle Medium (DMEM, Thermo Fisher Scientific, Waltham, MA, USA) containing 10% fetal bovine serum (FBS, Hyclone, Logan, UT, USA), 2 mM L-glutamine and antibiotics. HT-1080 (CCL-121, ATCC) cell line was maintained in Eagle's Minimum Essential Medium (MEM, Thermo Fisher Scientific) containing 10% FBS and supplemented with 2 mM L-glutamine, 1 mM sodium pyruvate, and antibiotics.

Generation of *LMNA* null cell line

A human lamin A Double Nickase Plasmid set (sc-400039-NIC, Santa Cruz Biotechnology, Dallas, TX, USA) was used to generate *LMNA*-knockout (LMNA_KO) cells. The lamin A Double Nickase Plasmid set consists of a pair of plasmids each encoding GFP/puromycin selection markers, and guide RNA (gRNA) sequences offset by approximately 20 bp to allow for specific Cas9-mediated double nicking of *LMNA* genomic DNA. Huh7 cells were transfected with the lamin A Double Nickase Plasmid set using Lipofectamine™ 2000

(Thermo Fisher Scientific) transfection reagent. Two days after the transfection, top 5% GFP-positive cells were sorted using a BD Influx (BD Biosciences, San Jose, CA, USA) cell sorter, and individual cells were plated into 96-well plates. Expression of lamin A/C in each single clone were determined by Western blot analysis and immunofluorescence staining using a lamin A/C antibody (ab108595, Abcam).

Antibodies and reagents

The manufacturers and dilutions of the antibodies used in Western blot analysis and immunofluorescence staining are listed in Supplementary Table S3 and Supplementary Table S4, respectively. TGFβ1 was obtained from PeproTech (Rocky Hill, NJ, USA); the TGFβ type I receptor/ALK5 inhibitor SB-431542 was purchased from TOCRIS (Bristol, UK). To induce EMT, cells were treated with 10 ng/mL TGFβ1 in completed medium containing 5% FBS.

Plasmids and transfection

Complementary DNA (cDNA) of human SMAD2 (Genbank: BC014840) was obtained from transOMIC Technologies (Huntsville, AL, USA), amplified by PCR, and cloned into pcDNA3 vector (Thermo Fisher Scientific) with two HA tags inserted at the C-terminus of

SMAD2 (i.e. SMAD2-HA). The nuclear-localizing green fluorescence protein (i.e. GFP-NLS) was constructed by inserting nuclear localization sequence (nucleotide sequence: 5'-ccaaagaagaaacgcaaagtg-3'; protein sequence: PKKKRKV) of SV40 Large T-antigen into 3' end of pEGFP-C2 (Clontech). The expression vector of CFP-H2B (pH2b-CyFP) and YFP-lamin B1 (pYFP-laminB1) were sourced from Jan Ellenberg [49]. The mCherry-H2B expression vector was modified from pH2b-CyFP by replacing CFP with mCherry cDNA. The mCherry-lamin A expression vector was obtained by cloning full-length lamin A into pZome-1-C vector with mCherry at 5' end driven by a CMV (cytomegalovirus) promoter. The GFP-lamin A expression vector was constructed by cloning GFP at the N-terminus of lamin A in pcDNA3 vector. The Lipofectamine^{TM} 2000 (Thermo Fisher Scientific) transfection reagent was used to deliver the expression plasmids into cells in accordance with the protocol provided by the manufacturer.

siRNAs and transfection

Sequences and/or manufacturers of the small interfering RNAs (siRNAs) used to deplete the expression of the targeted genes are listed in Table S5. Cells were transfected with siRNAs via Lipofectamine^{TM} RNAiMAX (Thermo Fisher Scientific) in accordance with the manufacturer's protocol.

RNA extraction and real-time quantitative PCR (qRT-PCR)

Total mRNAs were isolated from cells using RNeasy mini kit (Qiagen, Hilden, Germany). Complementary DNAs were produced using the SuperScript® IV Reverse Transcriptase system (Thermo Fisher Scientific). qRT-PCR was carried out using Power SYBR Green master mix (Thermo Fisher Scientific). The qRT-PCR primers of H3.3 (i.e. *H3-3A* gene) was obtained from Qiagen (Cat. No. QT00247128). Gene expression levels were normalized to *GAPDH* using primers (forward: 5'-GGAAGGTGAAGGTCGGAGTCA-3' and reverse: 5'- GTCATTGATGGCAACAATATCCACT-3').

Immunoblotting

Expression of proteins in cells were analyzed by Western blotting against specific antibodies summarized in Supplementary Table S3. Cells were lysed with RIPA buffer [50 mM HEPES, pH 7.3, 150 mM NaCl, 2 mM EDTA, 20 mM β-gylcerophosphate, 0.1 mM Na_3VO_4, 1mM NaF, 0.5 mM DTT and protease inhibitor cocktail (Roche Applied Science, Indianapolis, IN, USA)] containing 0.5% NP-40 with mild sonication in order to extract nuclear envelope and chromatin proteins. Total cell lysates were further lysed in 1× SDS sample buffer containing β-mercaptoethanol, analyzed by SDS-PAGE, transferred to

polyvinylidene fluoride (PVDF, Millipore) membranes, and blotted with primary antibodies. Corresponding horse radish peroxidase (HRP) or alkaline phosphatase (AP)-conjugated secondary antibodies (Sigma-Aldrich) were added, and the blots were developed by chemiluminescence in accordance with the manufacturer's protocols.

Immunofluorescence staining and confocal microscopy

Cells were fixed in 4% paraformaldehyde for 30 minutes at room temperature and permeabilized with 0.5% Triton X-100 in phosphate buffered saline (PBS) for 30 minutes. For the immunofluorescence staining of histone H3.3, antigen retrieval was carried out by incubation in 100^{o}C citrate buffer (10 mM Citric Acid, pH 6.0) for 1 hour, followed by incubation in 1% Triton X-100/PBS for 20 minutes. After two washes with PBS, cells were applied with 1% bovine serum albumin (BSA, Sigma-Aldrich)/PBS for 30 minutes at room temperature to block non-specific bindings. Then cells were incubated with primary antibodies (Supplementary Table S4) diluted in PBS for 1.5 hours at room temperature. Fluorescent (Alexa-488, Alexa-568 or Alexa-633)-conjugated secondary antibodies (Thermo Fisher Scientific) at dilution 1/1000 were used for detection. For PLA experiments, cells seeded in 8-well chamber slides (Millicell EZ SLIDE, Millipore) were fixed with 4% paraformaldehyde in PBS for 15 minutes. Cells were permeabilized with 0.5% Triton X-

100 in PBS for 30 minutes, and blocked with the Duolink® Blocking Solution for 1 hour at 37 ºC. Primary antibodies diluted in Duolink® Antibody Diluent where applied, and the slide were incubated for 1.5 hours at room temperature. Detection of protein interactions was performed by following the manufacturer's (Sigma-Aldrich) instructions. Cell nuclei were counterstained with Hoechst 33342 (Thermo Fisher Scientific) and mounted on slides using Prolong Gold antifade reagent (Thermo Fisher Scientific). Images were recorded using a Leica TCS SP5 confocal microscope (Leica, Wetzlar, Germany) equipped with HyD (hybrid detector). For live cell imaging, cells were incubated in a humidified chamber maintained at 37 ºC and supplied with 5% CO_2 (CU-109, Live Cell Instrument, Korea). Images were processed using Imaris 7.3 software (Bitplane, Zurich, Switzerland) and MetaMorph® (Molecular Devices, San Jose, CA, USA).

Immunogold staining and transmission electron microscopy (TEM)

Cells seeded on ACLAR® film were fixed in a mixture containing 0.1% glutaraldehyde and 1% paraformaldehyde (Electron Microscopy Sciences, Hatfield, PA, USA) for 2 hours on ice. Crosslinking was quenched using 0.125 M glycine, followed by neutralization with 0.1 M ammonium chloride. Cells were treated with a series of cold methanol dilutions, and then embedded in LR-Gold reagent on a Leica EM AFS2 (Leica Microsystems, Wetzlar,

Germany). The embedded samples were stored in a humidity control box at room temperature. For immunogold labeling, ultrathin sections of LR-Gold embedded samples were mounted on 200 mesh nickel grids covered with carbon-backed formvar film. The grids were first incubated with 3% normal sheep serum in PBS at room temperature for 15 minutes, and incubated with a mouse anti-H1 antibody (sc-8030, Santa Cruz, Dallas, TX, USA) for 60 minutes. After 6 sequential washes with 1% normal sheep serum in PBS, the grids were incubated for 60 minutes with 18 nm gold-IgG complexes. The grids were washed sequentially with 1% normal sheep serum in PBS and 3% normal rat serum in PBS, followed by incubation with a rabbit anti-H3K27me3 antibody (#9733, Cell Signaling, Danvers, MA, USA) for 60 minutes. After another 6 sequential washes with 1% normal rat serum in PBS, the grids were incubated for 60 minutes with 12 nm gold-IgG complexes. Following another sequential wash with 1% normal rat serum in PBS, the grids were incubated with 3% normal donkey serum in PBS at room temperature for 15 minutes, and incubated with a goat anti-Lamin B antibody (sc-6217, Santa Cruz) for 60 minutes. After washes with 1% normal donkey serum in PBS, the grids were incubated for 60 minutes with 6 nm gold-IgG complexes. The grids were then washed sequentially with 1% normal donkey serum in PBS, followed by two washes with triple distilled water. Finally, the grids

were treated with 2% uranyl acetate and 30 mM lead citrate. The final immunogold labeled grids were examined and photographed using a FEI Tecnai T12 electron microscope.

Mass spectrometry

Spots excised from the Coomassie blue-stained SDS-PAGE were digested using MS grade Trypsin Gold (Promega, Madison, WI) overnight at 37 °C. The tryptic digests were extracted using 10 µL Milli Q water initially, followed by two extractions using a total of 20 µL 50% Acetonitrile/0.1% Trifluoroacetic acid. The combined extracts were dried in a vacuum concentrator, and then dissolved in 1 µL of 5% Acetonitrile/0.5% Trifluoroacetic acid. A Thermo Scientific™ Orbitrap Fusion™ Lumos™ Tribrid™ Mass Spectrometer (Thermo Fisher Scientific) was used to detect electrospray ionization (ESI)-MS/MS and higher energy collisional dissociation (HCD)-MS/MS peptide signals. The MS/MS signal was analyzed using the MASCOT search engine (www.matrixscience.com).

Calculation of axial ratio (AR)

Nuclear morphology was quantified by calculating the axial ratio (AR) of each nucleus, determined from the nuclear staining of Hoechst 33342 cells. A custom Matlab code was developed to trace the nuclear perimeter, and applied elliptical Fourier analysis (EFA) to

find the first 20 elliptic harmonics [17]. AR was defined as the sum of the axes from the first 20 ellipses normalized by the first ellipse, subtracted by one. AR represents deviations from a perfect elliptical shape where bigger ellipses from the later harmonics would result in a larger AR value.

Statistical analysis

Data and statistical analyses were performed using Microsoft Excel and Graphpad Prism software. Data were analyzed using two-tailed Student's t-test or Fisher's exact test. P-values below 0.05 were considered significant.

Ethics approval and consent to participate: Not applicable

Consent for publication: Not applicable

Availability of data and material: All data generated or analyzed during this study are included in this published article (and its supplementary information files).

Funding: This work was supported by grants from the Ministry of Science and Technology,

Taiwan (MOST 106-2311-B-400-001 and MOST 108-2320-B-400-006-MY3).

Competing interests: Authors declare no competing interests.

Authors' contributions: Y.H.C. designed the research, analyzed the data, and wrote the article. Y.H.C., W.P.W., M.C.H., and J.Y.W. prepared cells, performed confocal imaging, qRT-PCR, and Western blot analysis. G.G.L. performed immunogold staining and TEM imaging, and P.G.C. characterized the nuclear morphology.

Acknowledgements: The authors would like to thank H. J. Kung, S. K. Huang, H. C. Chen, H. J. Lo, J. Y. Liou and H. J. Li for their help in obtaining cells and reagents as well as helpful discussion. The authors acknowledge W. H. Lin and M. Y. Chien for his valuable help in imaging and Western blot analysis. The authors also acknowledge the assistance of staff members at the Optic Biology Core Lab of National Health Research Institutes, the mass spectrometry technical research services from National Taiwan University (NTU) Consortia of Key Technologies and NTU Instrumentation Center, and the Image Core of Institute of Molecular Biology, Academia Sinica for technical support.

References

1. Kadota K, Suzuki K, Colovos C, Sima CS, Rusch VW, Travis WD, et al. A nuclear grading system is a strong predictor of survival in epitheloid diffuse malignant pleural mesothelioma. Mod Pathol. 2012;25(2):260-71. doi: 10.1038/modpathol.2011.146.
2. Chi YH, Chen ZJ, Jeang KT. The nuclear envelopathies and human diseases. J Biomed Sci. 2009;16:96. doi: 10.1186/1423-0127-16-96.
3. Seaman L, Meixner W, Snyder J, Rajapakse I. Periodicity of nuclear morphology in human fibroblasts. Nucleus. 2015;6(5):408-16. doi: 10.1080/19491034.2015.1095432.
4. Chow KH, Factor RE, Ullman KS. The nuclear envelope environment and its cancer connections. Nat Rev Cancer. 2012;12(3):196-209. doi: 10.1038/nrc3219.
5. Webster M, Witkin KL, Cohen-Fix O. Sizing up the nucleus: nuclear shape, size and nuclear-envelope assembly. J Cell Sci. 2009;122(Pt 10):1477-86. doi: 10.1242/jcs.037333.
6. Skinner BM, Johnson EE. Nuclear morphologies: their diversity and functional relevance. Chromosoma. 2017;126(2):195-212. doi: 10.1007/s00412-016-0614-5.
7. Paonessa F, Evans LD, Solanki R, Larrieu D, Wray S, Hardy J, et al. Microtubules Deform the Nuclear Membrane and Disrupt Nucleocytoplasmic Transport in Tau-Mediated Frontotemporal Dementia. Cell Rep. 2019;26(3):582-93 e5. doi: 10.1016/j.celrep.2018.12.085.
8. Karoutas A, Szymanski W, Rausch T, Guhathakurta S, Rog-Zielinska EA, Peyronnet R, et al. The NSL complex maintains nuclear architecture stability via lamin A/C acetylation. Nat Cell Biol. 2019;21(10):1248-60. doi: 10.1038/s41556-019-0397-z.
9. Gruenbaum Y, Margalit A, Goldman RD, Shumaker DK, Wilson KL. The nuclear lamina comes of age. NatRevMolCell Biol. 2005;6(1):21-31.
10. Swift J, Ivanovska IL, Buxboim A, Harada T, Dingal PC, Pinter J, et al. Nuclear lamin-A scales with tissue stiffness and enhances matrix-directed differentiation. Science. 2013;341(6149):1240104. doi: 10.1126/science.1240104.
11. Burke B, Stewart CL. The laminopathies: the functional architecture of the nucleus and its contribution to disease. AnnuRevGenomics HumGenet. 2006;7:369-405.
12. van Tienen FHJ, Lindsey PJ, Kamps MAF, Krapels IP, Ramaekers FCS, Brunner HG, et al. Assessment of fibroblast nuclear morphology aids interpretation of LMNA variants. Eur J Hum Genet. 2019;27(3):389-99. doi: 10.1038/s41431-018-0294-0.
13. Burke B. CELL BIOLOGY. When cells push the envelope. Science. 2016;352(6283):295-6. doi: 10.1126/science.aaf7735.
14. Heldin CH, Moustakas A. Signaling Receptors for TGF-beta Family Members. Cold

Spring Harb Perspect Biol. 2016;8(8). doi: 10.1101/cshperspect.a022053.
15. Horie M, Saito A, Noguchi S, Yamaguchi Y, Ohshima M, Morishita Y, et al. Differential knockdown of TGF-beta ligands in a three-dimensional co-culture tumor-stromal interaction model of lung cancer. BMC Cancer. 2014;14:580. doi: 10.1186/1471-2407-14-580.
16. Rangamani P, Lipshtat A, Azeloglu EU, Calizo RC, Hu M, Ghassemi S, et al. Decoding information in cell shape. Cell. 2013;154(6):1356-69. doi: 10.1016/j.cell.2013.08.026.
17. Diaz G, Zuccarelli A, Pelligra I, Ghiani A. Elliptic fourier analysis of cell and nuclear shapes. Comput Biomed Res. 1989;22(5):405-14. doi: 10.1016/0010-4809(89)90034-7.
18. Burke B, Stewart CL. Life at the edge: the nuclear envelope and human disease. Nat Rev Mol Cell Biol. 2002;3(8):575-85.
19. Burke B. The nuclear envelope: filling in gaps. NatCell Biol. 2001;3(12):E273-E4.
20. De Vos WH, Houben F, Kamps M, Malhas A, Verheyen F, Cox J, et al. Repetitive disruptions of the nuclear envelope invoke temporary loss of cellular compartmentalization in laminopathies. Hum Mol Genet. 2011;20(21):4175-86. doi: 10.1093/hmg/ddr344.
21. Denais CM, Gilbert RM, Isermann P, McGregor AL, te Lindert M, Weigelin B, et al. Nuclear envelope rupture and repair during cancer cell migration. Science. 2016;352(6283):353-8. doi: 10.1126/science.aad7297.
22. Raab M, Gentili M, de Belly H, Thiam HR, Vargas P, Jimenez AJ, et al. ESCRT III repairs nuclear envelope ruptures during cell migration to limit DNA damage and cell death. Science. 2016;352(6283):359-62. doi: 10.1126/science.aad7611.
23. Shimamoto Y, Tamura S, Masumoto H, Maeshima K. Nucleosome-nucleosome interactions via histone tails and linker DNA regulate nuclear rigidity. Mol Biol Cell. 2017;28(11):1580-9. doi: 10.1091/mbc.E16-11-0783.
24. Nava MM, Miroshnikova YA, Biggs LC, Whitefield DB, Metge F, Boucas J, et al. Heterochromatin-Driven Nuclear Softening Protects the Genome against Mechanical Stress-Induced Damage. Cell. 2020. doi: 10.1016/j.cell.2020.03.052.
25. Bianchi A, Mozzetta C, Pegoli G, Lucini F, Valsoni S, Rosti V, et al. Dysfunctional polycomb transcriptional repression contributes to lamin A/C-dependent muscular dystrophy. J Clin Invest. 2020;130(5):2408-21. doi: 10.1172/JCI128161.
26. Cesarini E, Mozzetta C, Marullo F, Gregoretti F, Gargiulo A, Columbaro M, et al. Lamin A/C sustains PcG protein architecture, maintaining transcriptional repression at target genes. J Cell Biol. 2015;211(3):533-51. doi: 10.1083/jcb.201504035.
27. Fredriksson S, Gullberg M, Jarvius J, Olsson C, Pietras K, Gustafsdottir SM, et al.

Protein detection using proximity-dependent DNA ligation assays. Nat Biotechnol. 2002;20(5):473-7. doi: 10.1038/nbt0502-473.
28. Uhler C, Shivashankar GV. Nuclear Mechanopathology and Cancer Diagnosis. Trends Cancer. 2018;4(4):320-31. doi: 10.1016/j.trecan.2018.02.009.
29. Dreger M, Madrazo E, Hurlstone A, Redondo-Munoz J. Novel contribution of epigenetic changes to nuclear dynamics. Nucleus. 2019;10(1):42-7. doi: 10.1080/19491034.2019.1580100.
30. Lomakin AJ, Cattin CJ, Cuvelier D, Alraies Z, Molina M, Nader GPF, et al. The nucleus acts as a ruler tailoring cell responses to spatial constraints. Science. 2020;370(6514). doi: 10.1126/science.aba2894.
31. Venturini V, Pezzano F, Catala Castro F, Hakkinen HM, Jimenez-Delgado S, Colomer-Rosell M, et al. The nucleus measures shape changes for cellular proprioception to control dynamic cell behavior. Science. 2020;370(6514). doi: 10.1126/science.aba2644.
32. Shimi T, Pfleghaar K, Kojima S, Pack CG, Solovei I, Goldman AE, et al. The A- and B-type nuclear lamin networks: microdomains involved in chromatin organization and transcription. Genes Dev. 2008;22(24):3409-21. doi: 10.1101/gad.1735208.
33. Broedersz CP, Brangwynne CP. Nuclear mechanics: lamin webs and pathological blebs. Nucleus. 2013;4(3):156-9. doi: 10.4161/nucl.25019.
34. Funkhouser CM, Sknepnek R, Shimi T, Goldman AE, Goldman RD, Olvera de la Cruz M. Mechanical model of blebbing in nuclear lamin meshworks. Proc Natl Acad Sci U S A. 2013;110(9):3248-53. doi: 10.1073/pnas.1300215110.
35. Taimen P, Pfleghaar K, Shimi T, Moller D, Ben-Harush K, Erdos MR, et al. A progeria mutation reveals functions for lamin A in nuclear assembly, architecture, and chromosome organization. Proc Natl Acad Sci U S A. 2009;106(49):20788-93. doi: 10.1073/pnas.0911895106.
36. Pan X, Chen Z, Huang R, Yao Y, Ma G. Transforming growth factor beta1 induces the expression of collagen type I by DNA methylation in cardiac fibroblasts. PLoS One. 2013;8(4):e60335. doi: 10.1371/journal.pone.0060335.
37. Van Berlo JH, Voncken JW, Kubben N, Broers JL, Duisters R, van Leeuwen RE, et al. A-type lamins are essential for TGF-beta1 induced PP2A to dephosphorylate transcription factors. Hum Mol Genet. 2005;14(19):2839-49. doi: 10.1093/hmg/ddi316.
38. Henikoff S, Smith MM. Histone variants and epigenetics. Cold Spring Harb Perspect Biol. 2015;7(1):a019364. doi: 10.1101/cshperspect.a019364.
39. Lin CJ, Conti M, Ramalho-Santos M. Histone variant H3.3 maintains a decondensed chromatin state essential for mouse preimplantation development. Development.

2013;140(17):3624-34. doi: 10.1242/dev.095513.
40. Banaszynski LA, Wen D, Dewell S, Whitcomb SJ, Lin M, Diaz N, et al. Hira-dependent histone H3.3 deposition facilitates PRC2 recruitment at developmental loci in ES cells. Cell. 2013;155(1):107-20. doi: 10.1016/j.cell.2013.08.061.
41. van Steensel B, Belmont AS. Lamina-Associated Domains: Links with Chromosome Architecture, Heterochromatin, and Gene Repression. Cell. 2017;169(5):780-91. doi: 10.1016/j.cell.2017.04.022.
42. Harr JC, Luperchio TR, Wong X, Cohen E, Wheelan SJ, Reddy KL. Directed targeting of chromatin to the nuclear lamina is mediated by chromatin state and A-type lamins. J Cell Biol. 2015;208(1):33-52. doi: 10.1083/jcb.201405110.
43. Gonzalez-Sandoval A, Gasser SM. On TADs and LADs: Spatial Control Over Gene Expression. Trends Genet. 2016;32(8):485-95. doi: 10.1016/j.tig.2016.05.004.
44. Hergeth SP, Schneider R. The H1 linker histones: multifunctional proteins beyond the nucleosomal core particle. EMBO Rep. 2015;16(11):1439-53. doi: 10.15252/embr.201540749.
45. Schlissel MS, Brown DD. The transcriptional regulation of Xenopus 5s RNA genes in chromatin: the roles of active stable transcription complexes and histone H1. Cell. 1984;37(3):903-13. doi: 10.1016/0092-8674(84)90425-2.
46. Brockers K, Schneider R. Histone H1, the forgotten histone. Epigenomics. 2019;11(4):363-6. doi: 10.2217/epi-2019-0018.
47. Fan Y, Nikitina T, Zhao J, Fleury TJ, Bhattacharyya R, Bouhassira EE, et al. Histone H1 depletion in mammals alters global chromatin structure but causes specific changes in gene regulation. Cell. 2005;123(7):1199-212. doi: 10.1016/j.cell.2005.10.028.
48. Alexandrow MG, Hamlin JL. Chromatin decondensation in S-phase involves recruitment of Cdk2 by Cdc45 and histone H1 phosphorylation. J Cell Biol. 2005;168(6):875-86. doi: 10.1083/jcb.200409055.
49. Beaudouin J, Gerlich D, Daigle N, Eils R, Ellenberg J. Nuclear envelope breakdown proceeds by microtubule-induced tearing of the lamina. Cell. 2002;108(1):83-96. doi: 10.1016/s0092-8674(01)00627-4.
50. Chen CY, Chi YH, Mutalif RA, Starost MF, Myers TG, Anderson SA, et al. Accumulation of the inner nuclear envelope protein sun1 is pathogenic in progeric and dystrophic laminopathies. Cell. 2012;149(3):565-77. doi: S0092-8674(12)00401-1 [pii];10.1016/j.cell.2012.01.059 [doi].

Figures and Legends

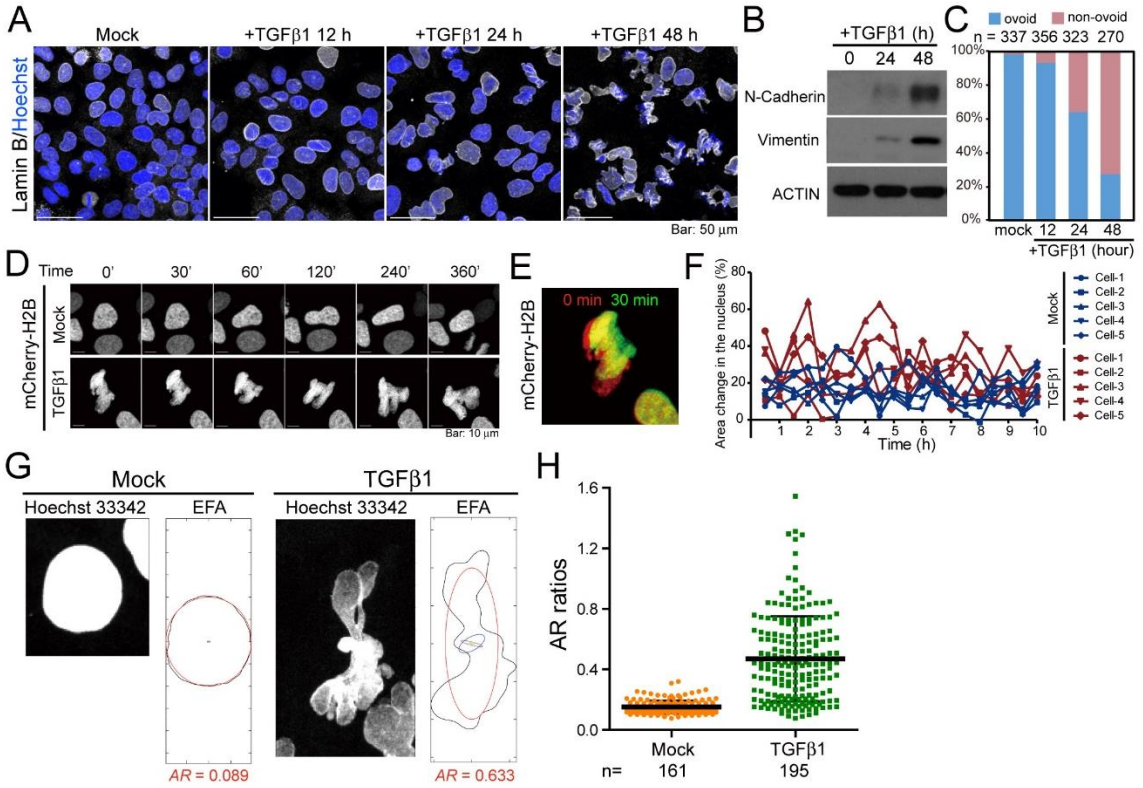

Figure 1. TGFβ1 induces nuclear deformation. (A) Confocal images of Huh7 cells with mock or with TGFβ1 treatment for 12 h, 24 h and 48 h. Cells were immunofluorescent stained with goat anti-lamin B (white). Nuclei were counterstained with Hoechst 33342 (blue). (B) Western blot analysis for the expression of mesenchymal markers N-Cadherin and Vimentin in Huh7 cells harvested after 0, 24 h, and 48 h of TGFβ1 treatment. ACTIN is a loading control. (C) Quantification of mock- and TGFβ1-treated cells, presenting as ovoid or non-ovoid, as shown in (A). Nuclei with more than two >240^{o} invaginations were identified as non-ovoid [50]. Number of cells quantified under each experiment condition was denoted. (D) Time-lapse confocal microscopic images of mCherry-tagged histone H2B (mCherry-H2B) in mock- and TGFβ1-treated Huh7 cells. Also see Supplementary movie S1 and movie S2. (E-F) Quantification of morphological changes (area in green divided by area in yellow+green) in the area of the nucleus in mock- and TGFβ1-treated cells every 30 min. Five cells were quantified under each condition. Percent area change is 15.72±0.78 in mock-treated and 24.66±1.278 in TGFβ1-treated cells. $P < 0.0001$, t-test. (G) Confocal images of nuclei stained with Hoechst 33342 (white, left images in each panel) and representative illustration of ellipse generation (right schemes in each panel, outlined by circles) by EFA to approximate the shape of the nucleus. The elliptic ARs increased with the curvature of the nucleus. (H) Quantification of ARs in Huh7 cells with mock or TGFβ1 treatment. Each dot represents one cell. More than 160 cells were quantified under each condition. $P < 0.0001$, t-test.

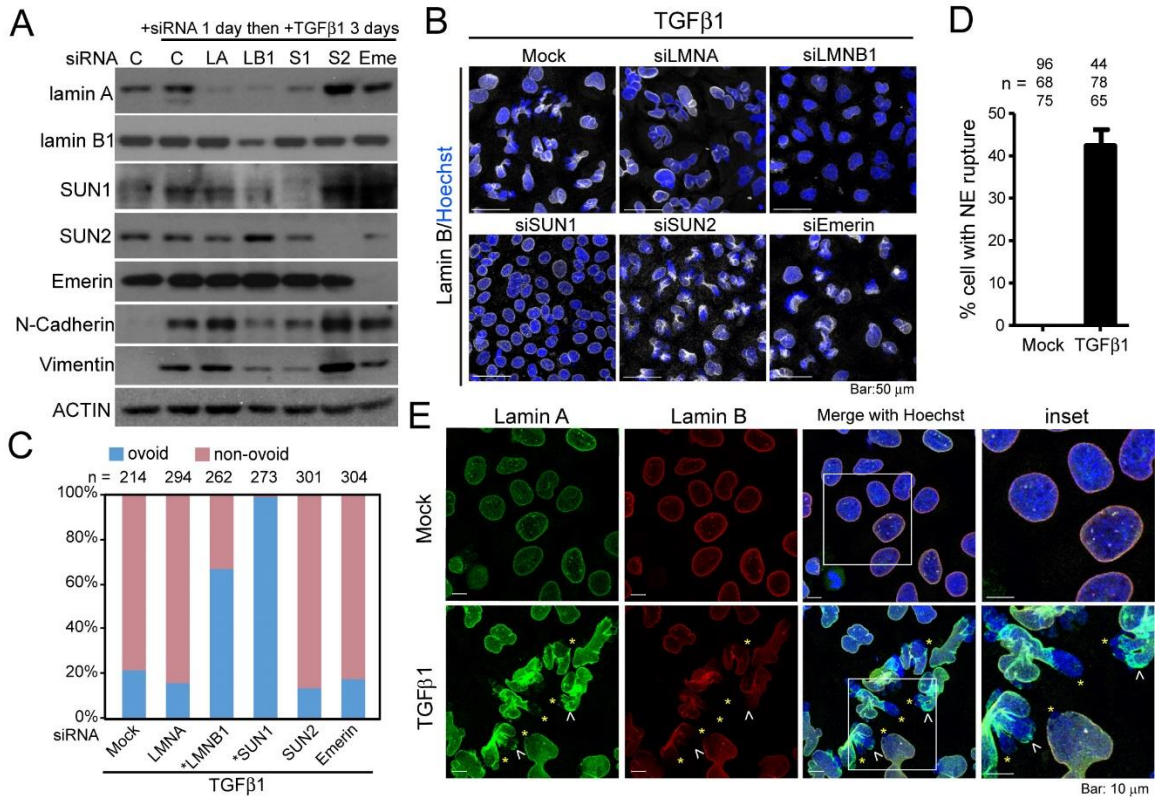

Figure 2. SUN1 and lamin B1, but not lamin A, contribute to TGFβ1-induced nuclear deformation. (A) Immunoblotting results of the indicated proteins in Huh7 cells transfected using the indicated siRNAs for 24 h then treated with 10 ng/mL TGFβ1 for three days. C, control; LA, lamin A; LB1, lamin B1; S1, SUN1; S2, SUN2; Eme, Emerin. ACTIN was used as a loading control. (B) Confocal images of cells transfected with the indicated siRNAs, followed by TGFβ1 treatment for 48 h. Cells were immunofluorescent stained with lamin B (white) and the nuclei were counter stained with Hoechst 33342 (blue). (C) Categorization of the nuclear shape in cells treated using the methods in (B). Number of cells quantified under each experiment condition was denoted. *, $P < 0.0001$, Fisher's exact test. (D) Quantification of mock- and TGFβ1-treated cells showing NE rupture. Results were averaged from experiments conducted in triplicate. (E) Confocal images of mock- and TGFβ1- treated Huh7 cells for 48 h. Cells were immunofluorescent stained using mouse anti-lamin A (green) and goat anti-lamin B (red). Nuclei were counterstained with Hoechst 33342 (blue). The yellow star indicates the NE stained negative for both lamin A and lamin B. The white arrow heads indicate the NE stained positive for lamin A and negative for lamin B. Insets: enlarged images indicated by white squares. Images in (B) and (E) are the sum of z-stacks.

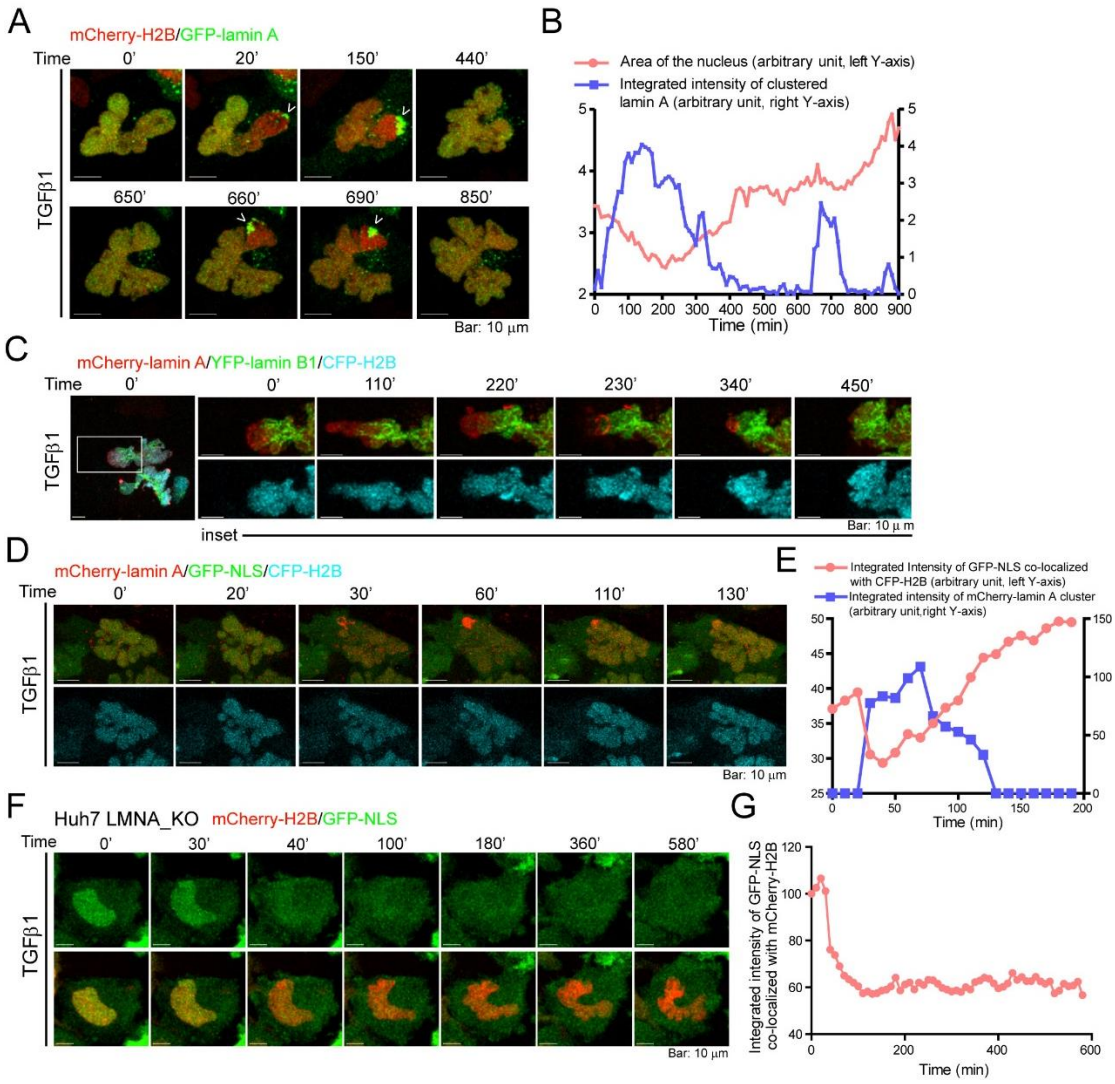

Figure 3. TGFβ1 induces rupturing and reformation of the NE. (A) Time-lapse imaging of GFP-Lamin A (green) and mCherry-H2B (red) under TGFβ1 treatment. The labeled time points are relative to the initial image, rather than the time after TGFβ1 addition. The white arrow head denotes GFP-lamin A clusters. See also Supplementary movie S3. (B) Quantification of nucleus area (denoted by mCherry-H2B, peach) and integrated intensity of GFP-lamin A cluster (medium blue) with time shown in (A) and Supplementary movie S3. (C) Time-lapse imaging of mCherry-lamin A (red), YFP-lamin B1 (green), and CFP-H2B (cyan) in Huh7 cells treated with TGFβ1. See also Supplementary movie S4. Insets: enlarged images showing the region outlined in the white square. (D) Time-lapse imaging of mCherry-lamin A (red), nuclear-localizing GFP (GFP-NLS, green), and CFP-H2B (cyan) in Huh7 cells treated with TGFβ1. See also Supplementary movie S5. (E) Quantification of integrated intensity of GFP-NLS co-localized with CFP-H2B (peach) and integrated intensity of mCherry-lamin A cluster (medium blue) as shown in (D). (F) Time-lapse imaging of mCherry-H2B (red) and GFP-NLS (green) in LMNA_KO Huh7 cells treated with TGFβ1. See also Supplementary movie S6. (G) Quantification of integrated intensity of GFP-NLS co-localized with mCherry-H2B as shown in (F). All images are the sum of z-stacks.

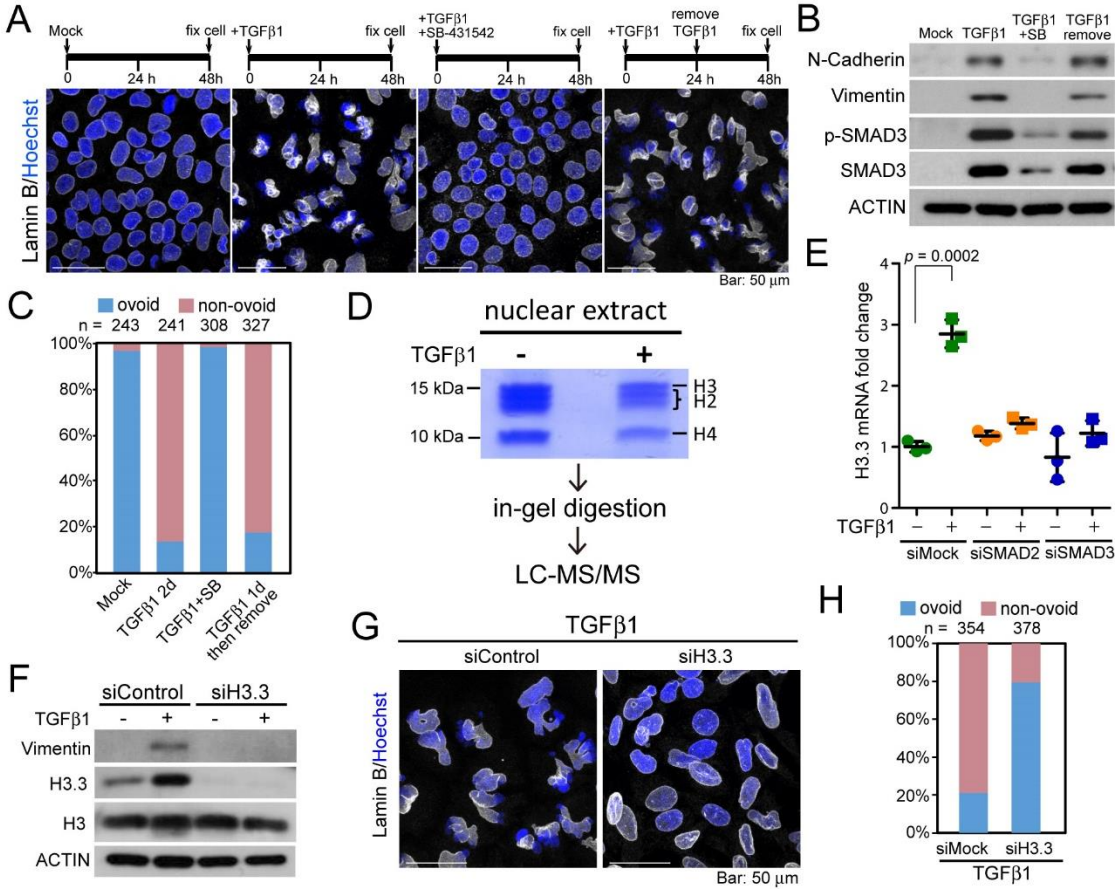

Figure 4. TGFβ1 provoked the transcription of histone H3.3, which contributed to nuclear deformation. (A) Morphology of the nucleus in Huh7 cells that underwent treatment in accordance with the schematic illustration presented above the confocal images. Cells were immunofluorescent stained using a lamin B antibody (white). Nuclei were counterstained with Hoechst 33342 (blue). (B) Western blot analysis for the expression of EMT markers in cells treated using the methods described in (A). SB, SB-431542 1 μM. (C) Categorization of nuclear shape in cells treated using the methods in (A). (D) SDS-PAGE stained with Coomassie blue for the nuclear extract from Huh7 cells without or with TGFβ1 treatment for 3 days. The histone H3 bands were excised, and subjected for in-gel digestion and LC-MS/MS analysis. (E) Quantitative RT-PCR for the relative mRNA expression levels of *H3.3* in mock- and TGFβ1-treated cells (for 72 h) pretreated with mock or SMAD2/SMAD3 siRNAs for 24 h. P value: t-test. (F) Western blot analysis for the expression of Vimentin, H3.3, and H3 in Huh7 mock- or H3.3 siRNA-treated, and induced to undergo EMT by TGFβ1 for 72 h. ACTIN immunoblotting was used as a loading control. (G) Morphology of nucleus as indicated by immunofluorescence staining of lamin B (white) in control and H3.3-depleted Huh7 cells treated with TGFβ1 for 48 h. Nuclei were counterstained with Hoechst 33342 (blue). Images are the sum of z-stacks. Categorization of the nuclear shape (ovoid or non-ovoid) is summarized in (H).

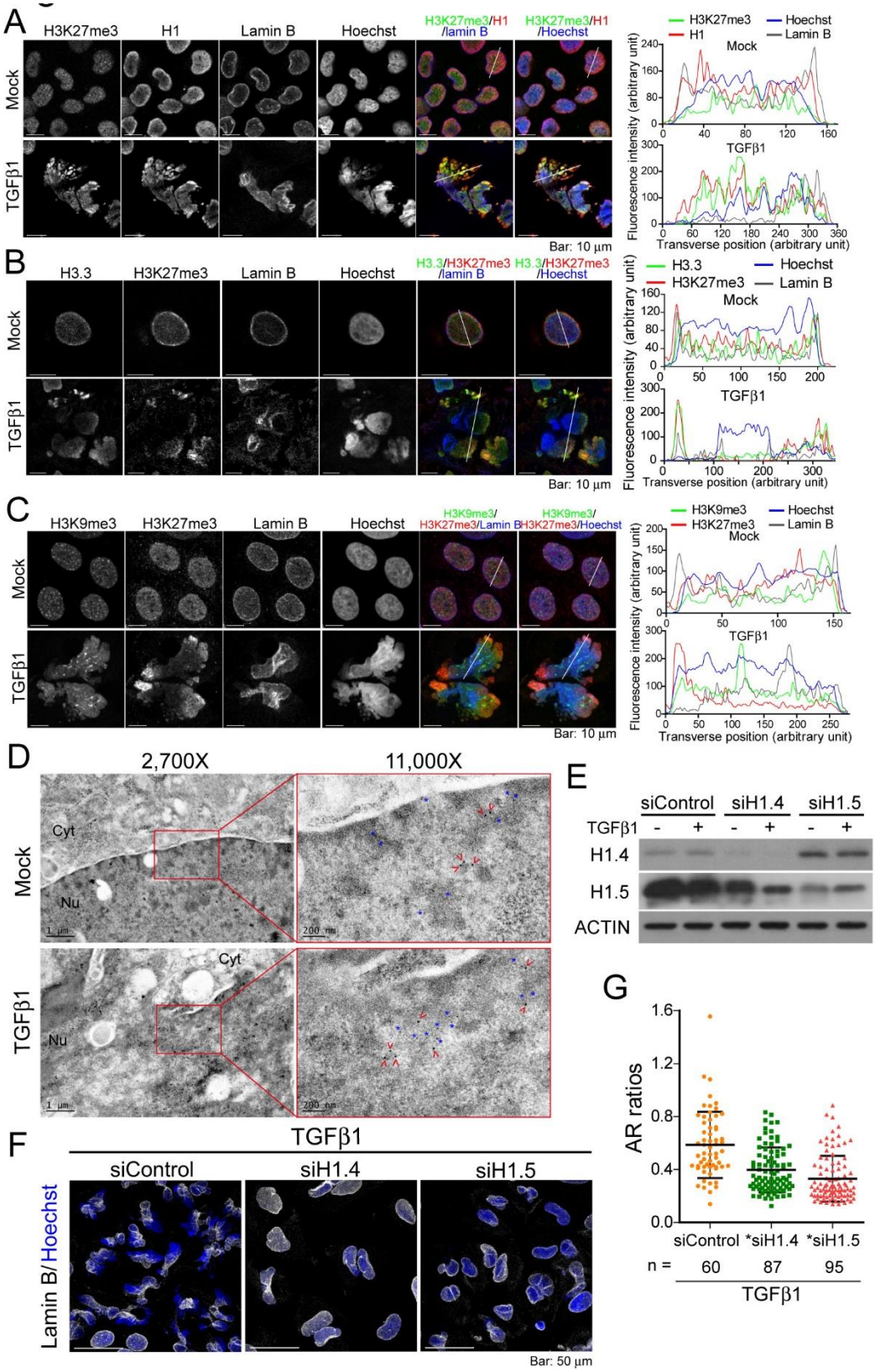
A
H3K27me3
H1
Lamin B
Hoechst
H3K27me3/H1 /lamin B
H3K27me3/H1 /Hoechst
Mock
TGFβ1
Bar: 10 μm
H3K27me3
H1
Hoechst
Lamin B
Fluorescence intensity (arbitrary unit)
Transverse position (arbitrary unit)
B
H3.3
H3K27me3
Lamin B
Hoechst
H3.3/H3K27me3 /lamin B
H3.3/H3K27me3 /Hoechst
Bar: 10 μm
C
H3K9me3
H3K27me3
Lamin B
Hoechst
H3K9me3/ H3K27me3/Lamin B
H3K9me3/ H3K27me3/Hoechst
Bar: 10 μm
D
2,700X
11,000X
Cyt
Nu
1 μm
200 nm
E
siControl
siH1.4
siH1.5
TGFβ1
H1.4
H1.5
ACTIN
F
TGFβ1
siControl
siH1.4
siH1.5
Lamin B/Hoechst
Bar: 50 μm
G
AR ratios
siControl
*siH1.4
*siH1.5
n =
60
87
95
TGFβ1

Figure 5. Chromatin status associated with NE rupture. (A) Confocal images of mock- and TGFβ1- treated cells immunofluorescence stained using H3K27me3, H1, and lamin B antibodies. Nuclei were counterstained with Hoechst 33342. (B) Confocal images of mock- and TGFβ1-treated cells immunofluorescent stained using H3.3, H3K27me3 and lamin B antibodies. (C) Relative distribution of the epigenetic marks H3K27me3, H3K9me3 and lamin B in mock- and TGFβ1-treated cells for 48 h. (A-C), single slice images. Transverse intensity line scans along the white lines in the corresponding cell images are presented on the right. (D) TEM images of mock- and TGFβ1-treated cells stained for H3K27me3 (12 nm gold-IgG, blue star), histone H1 (18 nm gold-IgG, red arrow head), and lamin B (6 nm gold-IgG, not denoted). Images are shown under 2,700× and 11,000× magnification. (E) Western blot analysis indicating the knocking down efficiency of H1.4 and H1.5 by siRNAs in Huh7 cells, followed by mock- or TGFβ1-treatment for 48 h. (F) Morphology of the nucleus in Huh7 cells depleted for H1.4 or H1.5, followed by TGFβ1 treatment for 48 h. Cells were immunofluorescent stained with lamin B (white). Nuclei were counterstained with Hoechst 33342 (blue). Images are the sum of z-stacks. (G) Quantification of elliptic ARs of the cells treated using the methods in (F). *, $P < 0.0001$, t-test.

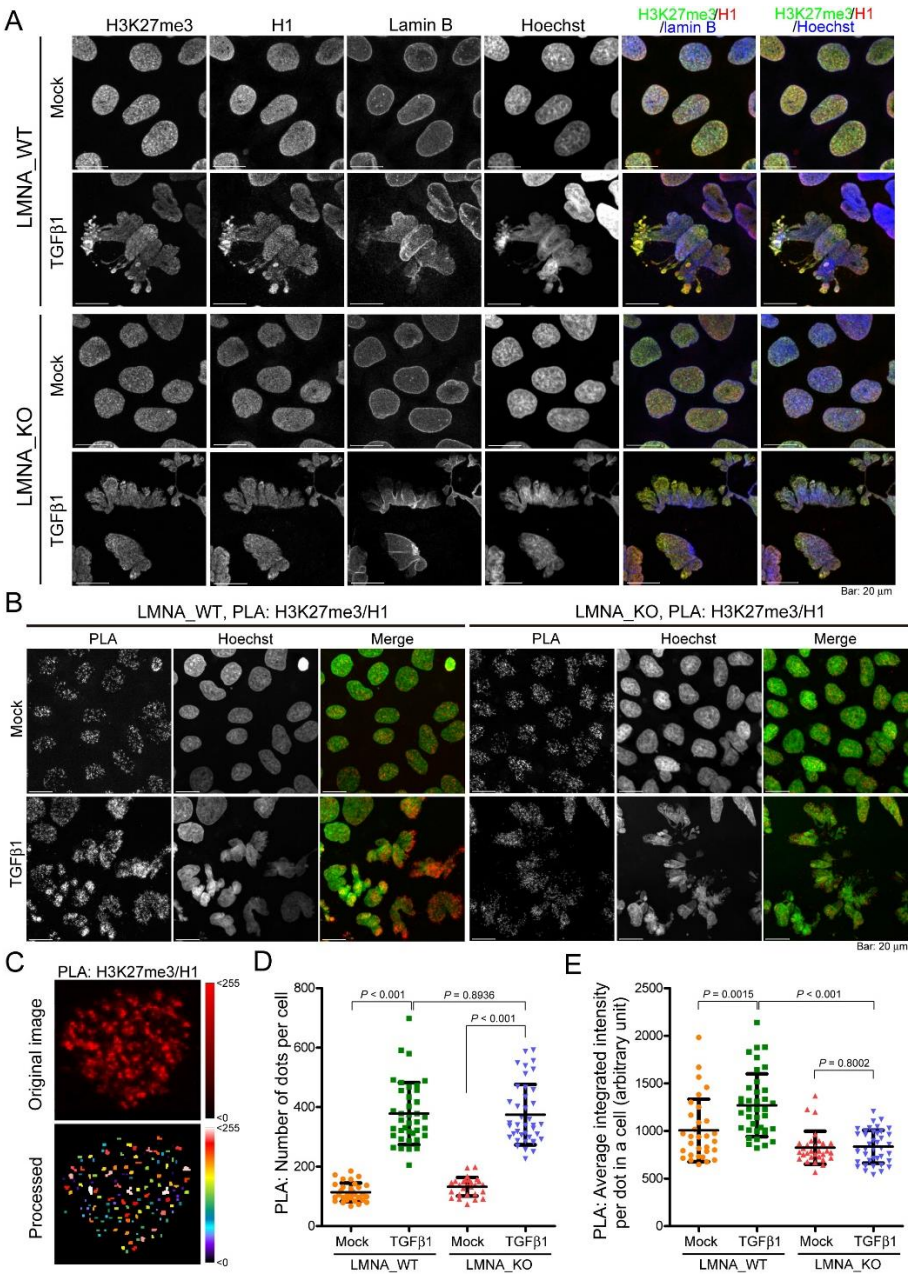

Figure 6. Depletion of *LMNA* reduced clustering of H3K27me3 and histone H1. (A) Representative confocal microscopy images of LMNA_WT and LMNA_KO Huh7 cells treated with/without TGFβ1 and immunostained using H3K27me3, H1, and lamin B antibodies, and Hoechst 33342. (B) Cells treated as described in (A) were subjected to PLA analysis. Each fluorescent dot represents the colocalization between H3K27me3 and histone H1. (C) Representative images showing the number and integrated intensity of the PLA fluorescent dots in a nucleus using MetaMorph® software; (upper) original fluorescence image; (lower) processed image. The average intensity of each dot is color-coded according to the scale on the right. (D) Number of PLA dots in each cell. (E) Average integrated intensity of each dot in each cell. Cell number calculations in (D) and (E) were: LMNA_WT, n=31; LMNA_WT + TGFβ1, N=38; LMNA_KO, n=30; LMNA_KO + TGFβ1, N=40. All images are the sum of z-stacks.

Figure 7

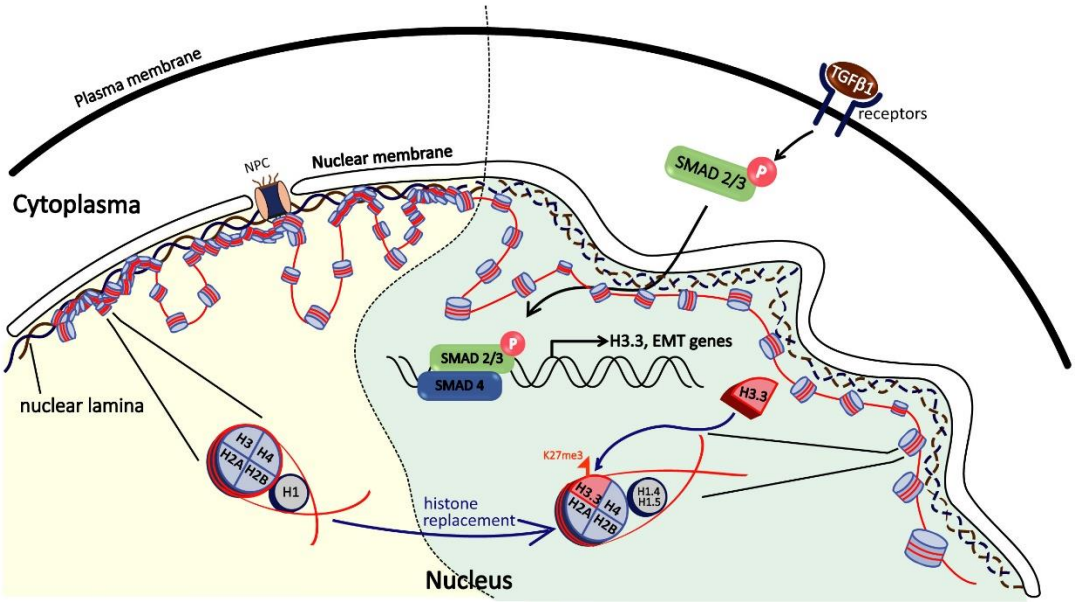

Figure 7. Schematics for the molecular events of the nuclear deformation induced by TGFβ1 stimulation. TGFβ1 treatment phosphorylates and activates the SMAD complex, thereby increasing transcription and the protein level of histone H3.3. The subsequent nucleosome incorporation of H3.3 may facilitate a dynamic chromatin environment that allows for further recruitment of histone H1.4/H1.5 variants, and the interaction with H3K27me3 for nuclear deformation and NE rupture.

Supplementary Tables, Figures and Movies

Table S1 LC-MS/MS quantification for the post-translation modification of histone H3 in Huh7.

Table S2 Relative abundance of histone variants in TGFβ1- versus mock- treated Huh7 cells.

Table S3 List of antibodies used in Western blot analysis.

Table S4 List of antibodies used in immunofluorescence staining.

Table S5 List of siRNAs.

Figure S1 TGFβ1 induces changes in nuclear morphology in multiple cell lines.

Figure S2 SUN1 and lamin B1 contribute to TGFβ1-induced nuclear deformation.

Figure S3 Expression and localization of NE proteins in TGFβ1-treated cells.

Figure S4 Examination of DNA damage response (DDR) in cells treated with TGFβ1.

Figure S5 TGFβ1-induced nuclear morphology change is a downstream process of SMAD signaling.

Figure S6 Association between variants and epigenetic status of histones with NE rupture.

Movie S1 Live-cell confocal imaging of the nucleus (denoted by mCherry-H2B) in Huh7 cells.

Movie S2 Live-cell confocal imaging of the nucleus (denoted by mCherry-H2B) in Huh7 cells treated with TGFβ1.

Movie S3 Live-cell confocal imaging of GFP-lamin A and mCherry-H2B in Huh7 cells treated with TGFβ1.

Movie S4 Live-cell confocal imaging of YFP-lamin B1 and mCherry-lamin A (A) combined with CFP-H2B channel (B) in Huh7 cells treated with TGFβ1.

Movie S5 Live-cell confocal imaging of GFP-NLS and mCherry-lamin A (A) combined with CFP-H2B channel (B) in Huh7 cells treated with TGFβ1.

Movie S6 Live-cell confocal imaging of GFP-NLS and mCherry-H2B in LMNA_KO Huh7 cells treated with TGFβ1.

Supplementary Tables

Table S1. LC-MS/MS quantification for the post-translation modification of histone H3 in Huh7.

Treatment	Protein Name	PTM	PTM Sequence	PTM spectrum (Count)
Mock	Histone H3.1			
		Acetyl (K)	**Total Acetyl sequences**	13
			K.STGGK#APR.K	3
			R.KQLATK#AAR.K	4
			R.K#SAPATGGVKKPHR.Y	1
			R.RYQK#STELLIR.K	3
			R.EIAQDFK#TDLR.F	1
			R.VTIMPK#DIQLAR.R	1
		Methyl (K)	**Total Methyl sequences**	9
			R.K#SAPATGGVKKPHR.Y	7
			K.SAPATGGVKK#PHR.Y	1
			R.EIAQDFK#TDLR.F	1
TGFβ1	Histone H3.3			
		Acetyl (K)	**Total Acetyl sequences**	5
			K.QLATK#AAR.K	2
			R.K#SAPSTGGVK.K	1
			R.EIAQDFK#TDLR.F	2
		Methyl (K)	**Total Methyl sequences**	2
			R.EIAQDFK#TDLR.F	2

Table S2. Relative abundance of histone variants in TGFβ1- versus mock- treated Huh7 cells.

Protein Name	Protein accession No.	Score Mascot	Protein coverage [%]	Relative abundance (TGFβ1/mock)
Histone H1.1	Q02539	67	7	1.786
Histone H1.2	P16403	67	13	1.331
Histone H1.3	P16402	67	12	1.331
Histone H1.4	P10412	67	12	1.331
Histone H1t	P22492	67	7	1.786
Histone H2A type 1-B/E	P04908	640	44	0.250
Histone H2A type 1-D	P20671	922	44	0.635
Histone H2A type 2-B	Q8IUE6	603	44	0.404
Histone H2A type 3	Q7L7L0	640	44	0.250
Histone H2A.V	Q71UI9	222	31	0.756
Histone H2A.Z	P0C0S5	222	31	0.756
Histone H2AX	P16104	687	45	1.105
Histone H2B type 1-A	Q96A08	768	43	1.245
Histone H2B type 1-B	P33778	3524	83	1.336
Histone H2B type 1-C/E/F/G/I	P62807	3633	75	1.699
Histone H2B type 1-D	P58876	3633	75	1.699
Histone H2B type 1-H	Q93079	3633	75	1.699
Histone H2B type 1-L	Q99880	3495	75	1.245
Histone H2B type 1-M	Q99879	3633	83	1.699
Histone H2B type 1-O	P23527	3523	75	1.336
Histone H2B type 2-E	Q16778	3523	75	1.336
Histone H2B type 2-F	Q5QNW6	3633	75	1.699
Histone H3.1	P68431	2536	89	0.984
Histone H3.1t	Q16695	2183	63	0.901
Histone H3.3	P84243	2207	89	2.571
Histone H3.3C	Q6NXT2	1265	45	1.153
Histone H3.Y	P0DPK2	563	12	1.307
Histone H3-like centromeric protein A	P49450	42	19	2.170
Histone H4	P62805	1450	62	0.354

Table S3. List of antibodies used in Western blot analysis.

Antibody	Make	Catalog No.	Dilution	Species
β-Catenin	Cell Signaling	#8480	1/2000	rabbit
N-Cadherin	Cell Signaling	#13116	1/1000	rabbit
Vimentin	Abcam	ab92547	1/10,000	rabbit
β-ACTIN	Sigma-Aldrich	A1978	1/100,000	mouse
SMAD3	Abcam	ab40854	1/10,000	rabbit
p-SMAD3 (Ser423+Ser425)	Abcam	ab52903	1/2,000	rabbit
SMAD2	Abcam	ab40855	1/2,000	rabbit
Lamin A	Millipore	MAB3540	1/5,000	mouse
Lamin A/C	Abcam	ab108595	1/5,000	rabbit
Lamin B1	Abcam	ab133741	1/10,000	rabbit
SUN1	Sourced from NIH (*13*)		1/5,000	rabbit
SUN2	Epitomics	5279-1	1/2,000	rabbit
Emerin	Santa Cruz	Sc-25284	1/5,000	mouse
Histone H3	Millipore	07-690	1/250,000	rabbit
Histone H3.3	Abcam	ab176840	1/5,000	rabbit
Histone H1.2	Abcam	ab181973	1/2,000	rabbit
Histone H1.3	Abcam	ab24174	1/1,000	rabbit
Histone H1.4	Invitrogen	703551	1/1,000	rabbit
Histone H1.5	Abcam	ab18208	1/2,000	rabbit
H3K27me3	Cell Signaling	#9733	1/2,000	rabbit

Table S4. List of antibodies used in immunofluorescence staining.

Antibody	Make	Catalog No.	Dilution	Species
Lamin B	Santa Cruz	sc-6217	1/300	goat
Lamin A	Millipore	MAB3540	1/300	mouse
Lamin A/C	Abcam	ab108595	1/500	rabbit
H3K27me3	Abcam	ab6002	1/200	mouse
H3K27me3	Cell Signaling	#9733	1/1,000	rabbit
Histone H1	Santa Cruz	sc-8030	1/600	mouse
Histone H3.3	Abcam	ab183902	1/500	rabbit
HA	Sigma-Aldrich	H6908	1/1,000	rabbit
SUN1	Sourced from NIH (*13*)		1/300	rabbit
NPC	Sigma-Aldrich	N8786	1/500	mouse
Emerin	Santa Cruz	sc-25284	1/100	mouse
H3K4me3	Cell Signaling	#9751	1/400	rabbit
H3K9me3	Abcam	ab8898	1/1,000	rabbit
H3K27me1	Abcam	ab194688	1/100	rabbit
H3K27me2	Cell Signaling	#9728	1/3,000	rabbit
H3K18ace	Cell Signaling	#13998	1/200	rabbit
H4K16ace	Millipore	07-329	1/500	rabbit

Table S5. List of siRNAs.

Gene	Target sequence	Make	Catalog No.
LMNA	AACTGGACTTCCAGAAGAACA	Qiagen	SI02654862
LMNB1	AACGCGCTTGGTAGAGGTGGA	Qiagen	SI00300671
SUN1	CCATCCTGAGTATACCTGTCTGTAT	Invitrogen	Hs_Sun1-2301
SUN2	AACCAAAGCAGGGTGGAATGTCTGC TGAAGAGGTCTTCTGAGTCTTGCTG	Invitrogen	Hs_Sun2-714 Hs_Sun2-1099
EMD (Emerin)	GCCTCCTCTTATAGCTTCTCTGACT	Invitrogen	HSS103213
H1-4 (H1.4)	N/A	Ambion	s6402
H1-5 (H1.5)	N/A	Ambion	s6405
H1-2 (H1.2)	N/A	Ambion	s6397
H1-3 (H1.3)	N/A	Ambion	s6398
H3-3A (H3.3)	CAGCGGTTCAACTTTATAATA ATACGTGGAGAACGTGCTTAA	Qiagen	SI04357514 SI04338152
SMAD2	CAGGTAATGTATCATGATCCA AAGCCGTCTATCAGCTAACTA	Qiagen	SI02757496 SI03033275
SMAD3	AGCCTATACTTTGGCAGGTTA AAGGAGCACCTTGACAGACTT AAGAGATTCGAATGACGGTAA ATCAAGGGATTTCCTATGGAA	Qiagen	SI05062645 SI00082502 SI00082495 SI00082481

N/A: not available

Supplementary Figures and Legends

Supplementary Figure S1

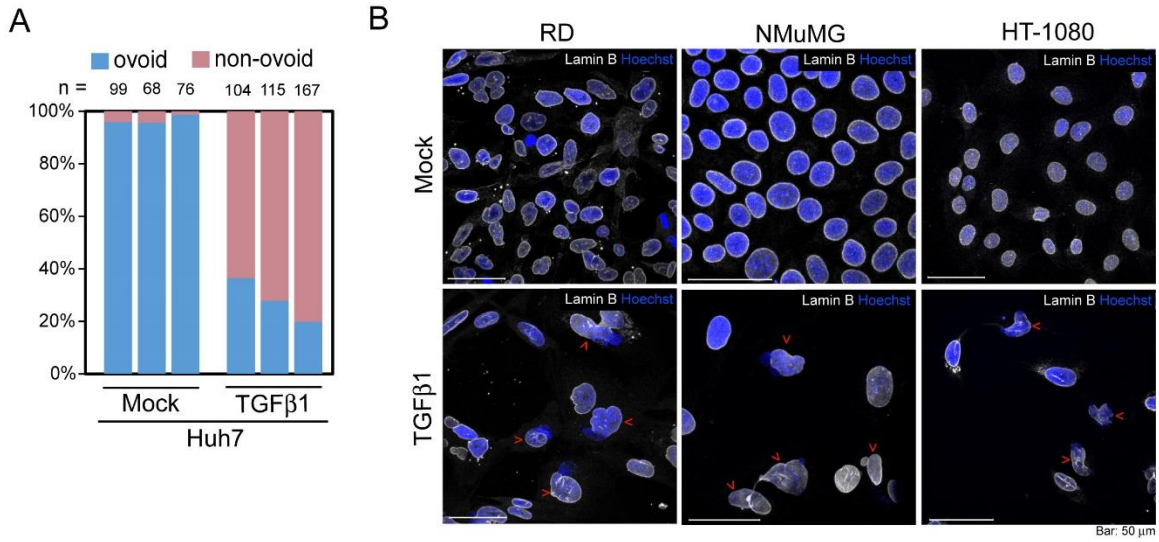

Supplementary Figure S1. TGFβ1 induces changes in nuclear morphology in multiple cell lines. (A) Characterization of the morphology (ovoid or non-ovoid) of cells treated with TGFβ1 or mock-treated. Number of cells quantified in experiments performed in triplicate was denoted. $P < 0.0001$ comparing mock- and TGFβ1-treated cells, Fisher's exact test. (B) Nuclear morphology of RD (human rhabdomyosarcoma), NMuMG (mouse mammary gland epithelial cell), and HT-1080 (fibrosarcoma) cells treated with 10 ng/mL TGFβ1 or mock-treated for 3 days. The red arrow heads denote cells with deformed nuclei. Cells were fixed using 4% paraformaldehyde and subjected to immunofluorescence staining with lamin B (white). The nuclei were counter stained with Hoechst 33342 (blue).

Supplementary Figure S2

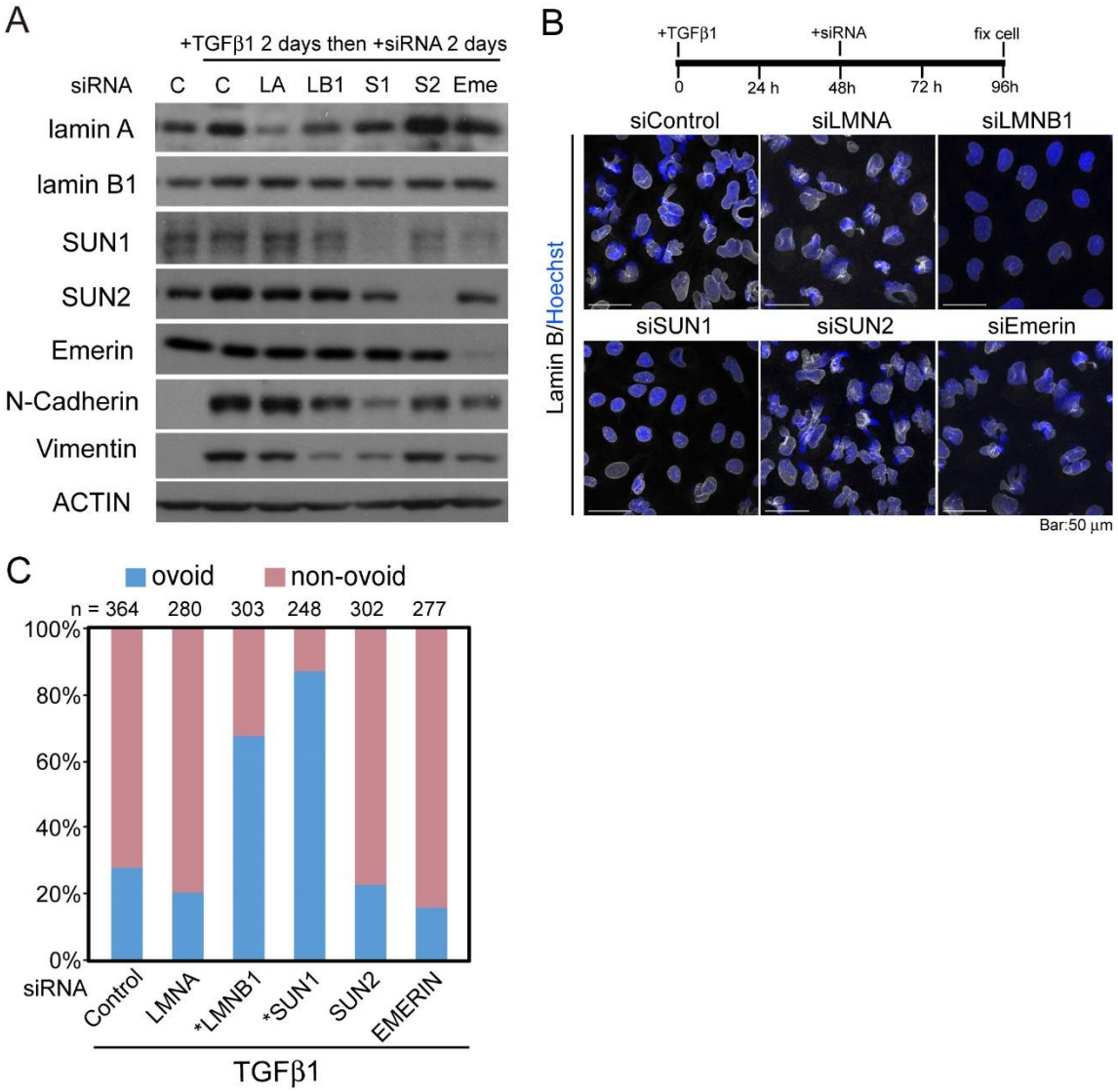

Supplementary Figure S2. SUN1 and lamin B1 contribute to TGFβ1-induced nuclear deformation. (A) Immunoblotting results of the indicated proteins in Huh7 cells first treated with TGFβ1 for two days, then transfected with the indicated siRNAs for another two days. (B) Cells were treated using the upper scheme, and were immunofluorescent stained with anti-lamin B (white). Nuclei were counterstained with Hoechst 33342 (blue). Images are the sum of z-stacks. (C) Quantification for the morphology (ovoid or non-ovoid) of cells treated using the methods in (B). Number of cells quantified under each experiment condition was denoted. *, $P < 0.0001$, Fisher's exact test.

Supplementary Figure S3

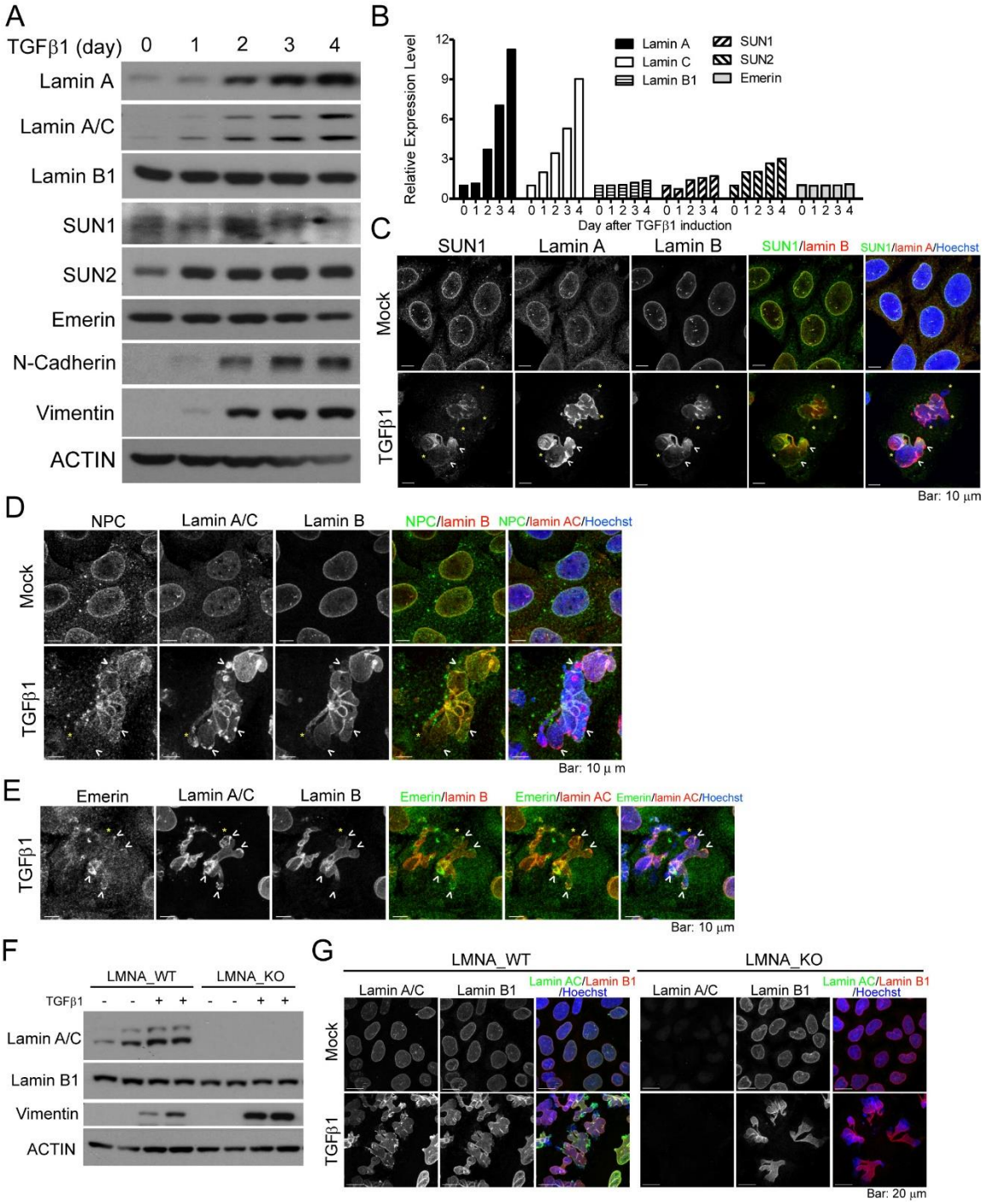

Supplementary Figure S3. Expression and localization of NE proteins in TGFβ1-treated cells. (A) Western blot analysis for the protein expression of nuclear lamins, NE proteins, and mesenchymal markers N-Cadherin and Vimentin in Huh7 cells harvested after TGFβ1 treatment for 0-4 days. ACTIN was used as a loading control. (B) Quantification of protein expression levels presented in (A). (C-E) Immunofluorescence staining images of Huh7 cells mock- or TGFβ1-treated for 2 days. The primary antibodies

were rabbit anti-SUN1, mouse anti-lamin A, goat anti-lamin B, mouse anti-nuclear pore complex (NPC, clone mAb414), rabbit anti-lamin A/C and mouse anti-Emerin. The yellow star indicates the NE stained negative for both lamin A and lamin B. The white arrow head indicates the NE stained positive for lamin A and negative for lamin B. Nuclei were counterstained using Hoechst 33342. (F) Western blot analysis for the expression of nuclear lamins and Vimentin in LMNA_WT and LMNA_KO Huh7 cells with/without TGFβ1 treatment for 72 h. Vimentin was used as a marker of EMT, and ACTIN is a loading control. (G) Confocal imaging of LMNA_WT and LMNA_KO Huh7 cells treated mock or TGFβ1 for 48 h, and immunofluorescent stained with lamin A/C and lamin B antibodies. Nuclei were counter stained with Hoechst 33342.

Supplementary Figure S4

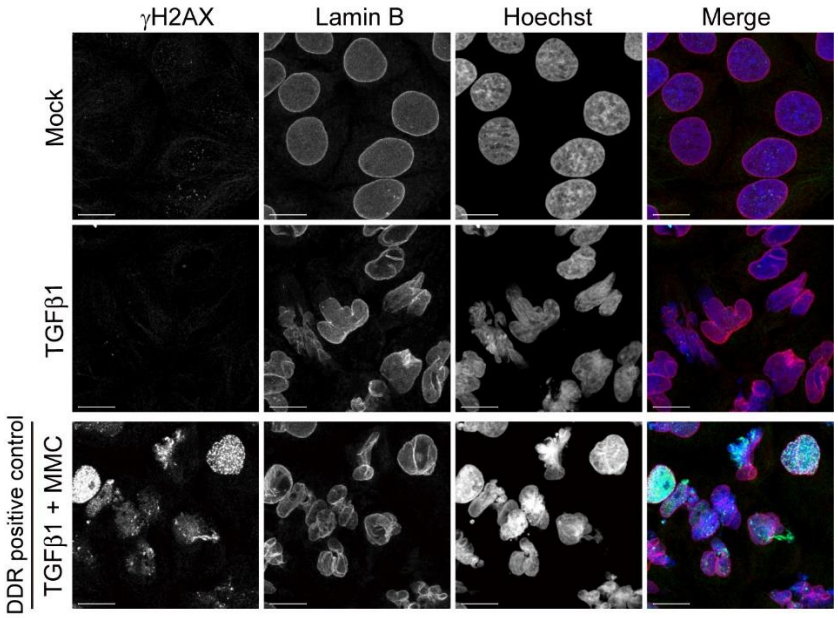

Supplementary Figure S4. Examination of DNA damage response (DDR) in cells treated with TGFβ1. Huh7 cells were either treated with mock, TGFβ1 for 48 h, or mitomycin-C (MMC, 5 ug/mL) for 24 h following the treatment of TGFβ1. Cells were fixed with 4% paraformaldehyde, and subjected for immunofluorescence staining with antibodies against γH2AX and lamin B. Nuclei were counter stained with Hoechst 33342. Scale bars: 20 μm. Images are the sum of z-stacks. Cells treated with MMC were used as a positive control for γH2AX immunofluorescence staining.

Supplementary Figure S5

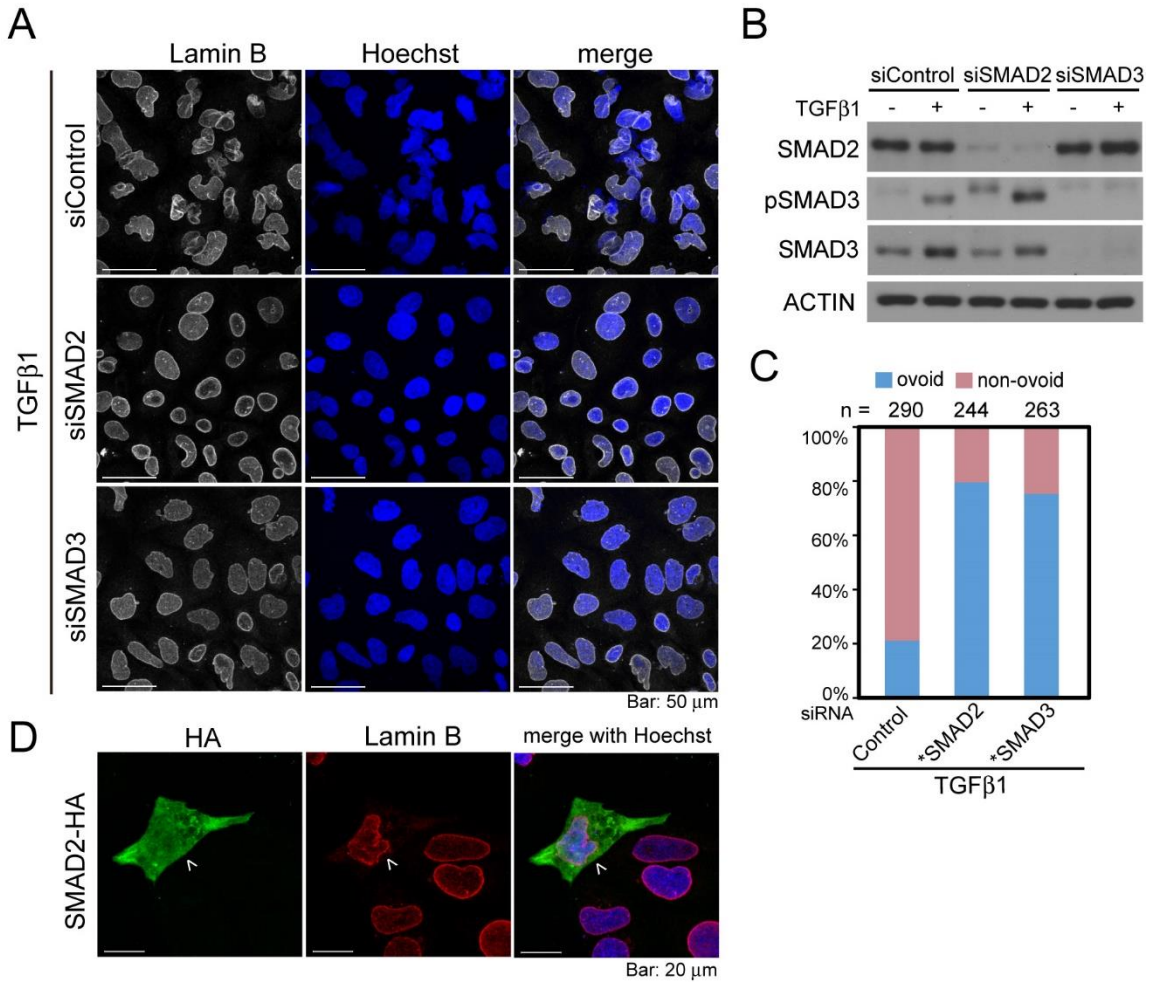

Supplementary Figure S5. TGFβ1-induced nuclear morphology change is a downstream process of SMAD signaling. (A) Confocal images of the nucleus in control, SMAD2 or SMAD3 siRNA-treated cells induced to undergo EMT by TGFβ1. Cells were fixed after 48 h of TGFβ1 treatment, and immunofluorescent stained using goat anti-lamin B (white). Nuclei were counter stained with Hoechst 33342 (blue). Images are the sum of z-stacks. (B) Western blot analysis for SMAD2 and SMAD3 in Huh7 cells treated using the methods in (A). ACTIN immunoblotting was used as a loading control. (C) Quantification of changes in the nuclear morphology (ovoid or non-ovoid) of cells treated with siRNAs respectively targeting SMAD2 and SMAD3, and induced to undergo EMT by TGFβ1 for 48 h. A total of 250-350 cells were quantified in each experiment. *, $P < 0.0001$, Fisher's exact test. (D) Confocal images of Huh7 cells transfected with a plasmid expressing HA-tagged SMAD2 (SMAD2-HA), and immunofluorescent stained with anti-HA (green) and anti-lamin B (red) antibodies. The white arrow head denotes a cell expressing SMAD2-HA. The nuclear morphology of the cell expressing SMAD2-HA is deformed (non-ovoid), whereas the un-expressed cells present an ovoid nuclear morphology. Nuclei were counter stained using Hoechst 33342 (blue). Images are the sum of z-stacks.

Supplementary Figure S6

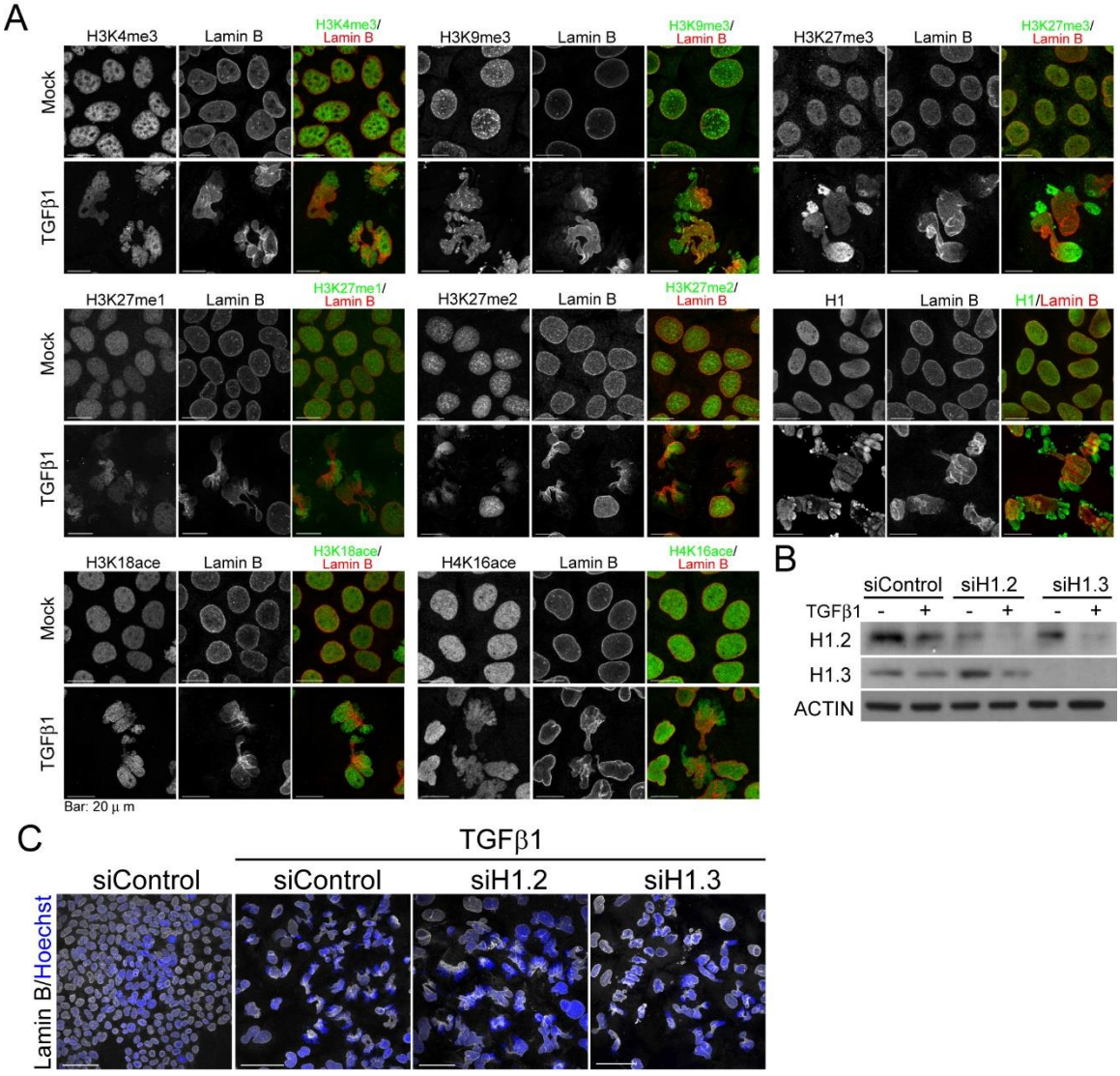

Supplementary Figure S6. Association between variants and epigenetic status of histones with NE rupture. (A) Relative distribution of the epigenetically modified histones and lamin B in mock- and TGFβ1-treated cells for 48 h. Cells were immunofluorescent stained using the indicated antibodies. Images are the sum of z-stacks. (B) Western blot analysis indicating the knocking down efficiency of H1.2 and H1.3 by siRNAs in Huh7 cells, followed by mock- or TGFβ1-treatment for 48 h. (C) Morphology of nucleus in Huh7 cells depleted for H1.2 or H1.3, followed by TGFβ1 treatment for 48 h. Cells were immunofluorescent stained with goat anti-lamin B (white). Nuclei were counterstained with Hoechst 33342 (blue). Images are the sum of z-stacks. Scale bars: 50 μm.

Supplementary Files

This is a list of supplementary files associated with this preprint. Click to download.

- MovieS6.mov
- movieS1.mov
- movieS2.mov
- movieS3.mov
- movieS4A.mov
- movieS4B.mov
- movieS5A.mov
- movieS5B.mov